IEEE Access
Multidisciplinary ⋮ Rapid Review ⋮ Open Access Journal

Received 2 February 2024, accepted 28 February 2024, date of publication 4 March 2024, date of current version 13 March 2024.

Digital Object Identifier 10.1109/ACCESS.2024.3372850

RESEARCH ARTICLE

PFPD_MCA: A Multiconductor Power Flow

LUCA RUSALEN, (Member, IEEE), AND ROBERTO BENATO, (Senior Member, IEEE)
Departement of Industrial Engineering, University of Padova, 35131 Padua, Italy
Corresponding author: Luca Rusalen (luca.rusalen@phd.unipd.it)

ABSTRACT In this paper, the multiconductor extension of the previously developed three-phase power flow algorithm (named PFPD_3P) is presented. This multiconductor formulation has a general validity for both distribution and transmission networks. An iterative matrix formulation for the solution is throughout expounded. The present method allows computing the electrical quantities of all the network conductors: the active conductors and the passive ones (*i. e.*, OHL ground wires, IC metallic screens/armours, and GIL enclosures). These electrical quantities can be evaluated both at the network busbars and also along the lines. The knowledge of these quantities can be useful to perform: safety evaluations, power quality and electromagnetic compatibility studies. The electrical substations are carefully modelled, by considering the links between the passive conductors of different busbars and the earthing resistance of the meshed earth electrode. The algorithm is implemented in Matlab environment and tested by several fictitious networks. Eventually, in order to confirm the approach accuracy, the multiconductor results are compared with the equivalent single-phase ones and the three-phase power flow commercial software DIgSILENT PowerFactory.

INDEX TERMS Multiconductor transmission lines, power flow, power system analysis, transmission network.

NOMENCLATURE

A. SETS AND INDICES

Symbol	Quantity
a	Slack-bus.
$b \div g$	Generator buses.
$h \div m$	Load buses.
G	Set of generator buses $a \div g$.
L	Set of load buses $h \div m$.
g	Generation busbar.
l	Load busbar.
$0, 1, \ldots k$	Initial, first, …, *k-th*iteration.
$\_q$	Quadrature component.
c	Corrected value.
k	*k-th* iteration.
t	Load typology.
$\underline{\boldsymbol{Y}}, \underline{\boldsymbol{Y}}_N, \underline{\boldsymbol{Y}}_{SGL}, \underline{\boldsymbol{Y}}_P$	Total bus admittance, network admittance, shunt admittance, primitive admittance matrices.
$\underline{\boldsymbol{Y}}_{GG}, \underline{\boldsymbol{Y}}_{GL}, \underline{\boldsymbol{Y}}_{LG}, \underline{\boldsymbol{Y}}_{LL}$	Admittance submatrices of $\underline{\boldsymbol{Y}}$.
$\underline{\boldsymbol{Y}}_{Geq}$, $\underline{\boldsymbol{Z}}_{Geq}$	Admittance and impedance equivalent matrices as seen at generator busses.
$\underline{\boldsymbol{T}}_x$	Transformation matrix.
$\underline{\boldsymbol{F}}$	Generalized Fortescue transformation matrix.
$\boldsymbol{R}$	Passive conductor reduction matrix.
$\boldsymbol{I}$	Identity matrix.
$\boldsymbol{S}$	Incidence matrix.
ABC	Phase frame of reference.
ABCM	Multiconductor frame of reference.
0PN	Sequence frame of reference.
0	Zero sequence component.
P	Positive sequence component.
N	Negative sequence component.

B. VARIABLES AND PARAMETERS

$\underline{u}$	Complex voltage.
$\underline{\boldsymbol{u}}$	Complex voltage vector.
$\lvert\underline{u}\rvert$	Voltage magnitude.
δ	Voltage angle.
$\underline{i}$	Complex current.
$\underline{\boldsymbol{i}}$	Complex current vector.
$\Delta\underline{\boldsymbol{i}}$	Correcting current vectors.

The associate editor coordinating the review of this manuscript and approving it for publication was Fabio Mottola.

$\underline{y}$	Complex admittance.
$\underline{s}$	Complex power.
p	Active power.
q	Reactive power.
Δ	Elementary cells length.
ρ_E	Substation soil resistivity.

C. SYMBOLS

^{T}	Transposition.
$*$	Complex conjugate.
$^{-1}$	Matrix inversion.
$\div$	From . . . to . . .
$\otimes$	Hadamard element-wise multiplication
$\odot$	Block-wise multiplication
$/$	Element-wise division
Im	Imaginary part of a complex quantity

D. ACRONYMS

OHL	**O**ver **H**ead **L**ine.
IC	**I**nsulated **C**able.
GIL	**G**as **I**nsulated **L**ine.
MCA	**M**ulticonductor **C**ell **A**nalysis.
PFPD	**P**ower **F**low of the University of **Pad**ova.
PFPD_3P	**P**ower **F**low of the University of **Pad**ova **3 P**hase.
PFPD_MCA	**P**ower **F**low of the University of **Pad**ova together with the **M**ulticonductor **C**ell **A**nalysis.
DGS	**DI**g**S**ILENT PowerFactory.
DSO	**D**istribution **S**ystem **O**perator.
TSO	**T**ransmission **S**ystem **O**perator.

I. INTRODUCTION

A. MOTIVATION

Nowadays, power flow study is one of the most relevant tools to assess power systems operation and planning. The aim of these studies is to compute the voltage (in magnitude and phase) at each busbar of the grid. Starting from the voltage solutions, the currents flowing in all the elements of transmission network can be evaluated. During decades of research, different approaches have been developed to solve power flows (Newton-Raphson, decoupled, fast-decoupled). A great part of these methods has been applied to solve the equivalent single-phase circuit at the positive sequence, since the system unbalances are ignored. However, in distribution/transmission systems, it is unfeasible to completely balance the loads, or to achieve perfectly symmetric transmission lines, as a consequence of the rarely transposed high voltage lines. To perform a realistic assessment of these systems, different three-phase power flow algorithms have been developed. Three-phase approach only represents the three active conductors of the power systems.

This paper proposes an innovative procedure to investigate unbalanced system power flows, by considering both the active conductors and the passive conductors. The term active conductor is adopted as synonymous of live conductor, which is a conductor intended to be energized in normal operation. Instead, the passive conductors are all the other line conductors (such as earth wires of OHLs, screens and armours of IC lines, enclosures of GILs); the aim of these conductors is to guarantee a reliable line operation.

For the first time in technical literature, the knowledge of the electric quantities in all the system conductors (active and passive ones) allows performing safety and electromagnetic interference evaluations. For instance, it is possible to assess: the magnitudes of the passive conductor contact voltages (fundamental for live line works), the ground return current (fundamental for electromagnetic interferences), the magnetic fields produced by the currents circulating in all the conductors.

B. LITERATURE REVIEW

For most purposes in the steady-state analysis of power systems, the system unbalances can be neglected and the equivalent single-circuit at the positive sequence can be adopted to solve the power flows. Through the years, the power flow problem has represented a cornerstone of network steady-state operation and planning. Moreover, the increase of grid extension causes a growing of the power-flow problem dimensions. In order to make the issue sustainable from a computation standpoint, different approaches have been developed to solve equivalent single-circuit at the positive sequence. Some of these are: linear equations [1], fast-decoupled [2], conic format [3], convex relaxation [4] and quadratic conic relaxation [5]. The aim of fast-decoupled method [2] is to decrease the computational cost for large transmission networks, in which $r/x \ll 1$. Instead, in other approaches the goal is to develop a robust algorithm to solve the ill-conditioned networks [3], [4], [5].

If the system unbalance cannot be ignored, three-phase power flow must be applied. Different solution approaches have been developed: they can be divided in three categories. The first exploits an approach based on phase frame of references [6], [7], [8], [9], and [10], so all the grid elements are modelled by means of their phase matrices. The second is based on the symmetrical frame of reference and in order to model the asymmetrical devices (where the three single-phase sequence circuits are mutually coupled) suitable compensation techniques are implemented [11], [12], [13], [14]. These techniques symmetrize the asymmetrical components and the power flow problem can be solved by studying the three single-phase sequence circuits separately. The latter category is based on a hybrid technique [15], [16], [17], where each iterative cycle alternates the use of both the phase frame of reference and the symmetrical frame of reference.

For the distribution networks, which are typically unbalanced, specific approaches and open-source toolboxes have been developed. These algorithms are designed to consider

the neutral conductor presence, given that in low-voltage distribution networks the single-phase loads are connected between a phase conductor and the neutral conductor. In fact, the neutral current might be larger than the phase currents if the loads are strongly unbalanced. Furthermore, different neutral designs must be considered, since the design varies from country to country: networks without neutral, networks with an isolated neutral, networks with multiple neutral grounding, networks with resistance neutral grounding and networks with neutral compensated via Petersen coil.

In the last decades, different approaches have been presented in literature for distribution systems: backward-forward sweep technique [18], [19], Newton-Raphson method [20], [21], current injection method [22], [23] and Holomorphic embedding load flow [24]. In order to solve the unbalanced power flow problem, some approaches have been developed specifically for distribution networks [25], [26]. Eventually, some open-source toolboxes have been developed to solve power-flow of distribution networks, two of these are OpenDSS [27] and PowerModelsDistribution. All the mentioned methods allow considering the neutral conductor in the distribution line model, but the passive conductors (such as earth wires of OHLs, screens and armours of IC lines, enclosures of GILs) cannot be considered.

With regard to the line passive conductors, some approaches do not consider their effects and the lines are represented by neglecting their presence on the transmission lines [11], [12], [13], [14], [15], [16]. More precise methods [17] embed the passive conductor effects into the active conductors by exploiting the Kron's matrix reduction [28]. However, the reduction technique can be applied if some hypotheses are verified (i.e., either the voltages or alternatively the currents of the passive conductors at the ends of the electric line are null). In real power systems, these hypotheses are not always verified. In any case, the simplifying hypotheses introduce ''light'' approximations in the three-phase power flow results.

A very precise steady-state regime evaluations on the passive conductors can be performed by means of multiconductor approach, which assesses all the electric quantities of all the conductors and hence the ground return current. In the past decades, different methods have been presented in literature [29], [30], and [31]; in all these methods, the sending-end of the transmission line is supplied by a three-phase voltage source, and, at the receiving-end, a load is applied. This is a powerful circuital tool, but not a power flow approach since the considered line is evaluated as stand-alone from the network. Furthermore, in the present method, at the sending and receiving ends, the passive conductors are connected to the substation grounding system. The substation grounding system is connected to the passive conductors of all the transmission lines reaching the substation, so the power systems passive conductors constitute a meshed grid. The electrical quantities of the passive conductors cannot be evaluated with the above-mentioned methods.

C. CONTRIBUTIONS

The paper demonstrates how the power flow problem can be solved by considering the power system multiconductor representation. Differently from the other power flow methods, this multiconductor formulation allows evaluating the power flow of any grid without any simplifying hypothesis. The present algorithm puts together two open powerful tools of power systems analysis: the Multiconductor Cell Analysis (MCA) and the three phase Power Flow of the University of Padova (PFPD_3P) [17] in fact, it is named PFPD_MCA.

The specific contributions are the following:

- A novel hybrid algorithm (phase/sequence frame of reference) to solve power flow in unbalanced multiconductor power systems;
- This method can be also applied to evaluate both the power quality (*i.e.*, the electric quantity unbalances) and the electromagnetic interference.

Differently from the previous method PFPD_3P, where the passive conductor effects are englobed inside the active ones by exploiting the Kron's matrix reduction technique, in PFPD_MCA the passive conductors are stored in the admittance matrix representing the network. Hence, no simplifying hypotheses or approximations are introduced.

The proposed approach is completely general and due to MCA formulation, each transmission line technology can be modelled: OHL (both single and double circuit) with any number of earth wires, land or submarine, single-core or three-core IC lines (with screens and armours) and GIL. Each line is represented by considering its real laying configuration and conductor characteristics. The method allows considering any IC screen arrangements: single point-bonding, cross-bonding, solid-bonding and multiple-point solid-bonding. The proposed solution is as simple as effective, and it can be applied both to distribution and transmission network.

The power quality is assessed with regard to the electric quantity unbalance factors. In fact, the voltage unbalance may lead to the onset of unwanted phenomena like untimely grid protection interventions, and electrical machine overheating, which cause a systematic lowering in reliability, quality, and efficiency of the entire power system. Regarding the electromagnetic interferences, starting from the unbalance power flow results, this method can compute the external magnetic fields along all the line route (also including the currents in the passive conductors) and also the ground return current.

The effectiveness of the proposed method is thoroughly tested by considering different networks. These networks have different extensions (in busbar number and line lengths) and line technologies.

In order to confirm the method effectiveness, all the analysed networks are also tested in the equivalent single-phase circuit at the positive sequence [32].

From the knowledge of the phase voltages in all the busbars of the considered network, it is possible to completely assess the behaviours of the electrical quantities also along the lines. These quantities can be exploited to estimate the impact of

the electrical lines on the territory in terms of electromagnetic compatibility.

D. PAPER ORGANIZATION

The remainder of the paper is organized as follows. Section II outlines the algorithm adopted to assess multiconductor power flow. Section III presents the model implemented to consider the connection between the passive conductors of different lines that arrive at the same substation. In Section IV, two case studies are presented. The former evaluates the multiconductor power flow of a 18-busbar network, and the latter a 39-busbar network. The multiconductor results are compared with the equivalent single-phase circuit at the positive sequence ones and with the commercial software DGS. The DGS software implements the Newton-Raphson method to compute the three-phase power-flow solution. The passive conductor effects are included into the passive ones by exploiting the Kron's matrix reduction technique. Section V draws conclusions and outlines future works.

II. METHOD FORMULATION

This section presents the iterative procedure to assess the power flow in unbalanced multiconductor networks. Two years ago, the authors published an AC three-phase power flow algorithm (named PFPD_3P) based on a three-phase ''all-inclusive'' bus admittance matrix. The ''all-inclusive'' bus admittance matrix stores all the unbalanced power flow data (*i. e.*, the grid structure and the bus constraints). Therefore, a concise, efficient, and rapid algorithm to solve unbalanced power flow has been presented [17].

The reason that drives the authors to make research on this topic is understanding if the three-phase unbalanced power flow algorithm PFPD_3P could be extended to assess also the multiconductor power systems. The innovation introduced by the present approach is the assessment of the passive conductor electrical quantities both at all the network busbars and also along the electrical lines. Before starting to introduce the iterative procedure, it is fundamental to report what the term ''multiconductor'' means: in this power flow approach, beyond the three active conductors, also the passive conductors are modelled, in both the electrical lines and the substations. The passive conductors in a power system are the ground wires of OHLs, the IC metallic screens, the enclosures of GILs and neutral conductor of distribution lines. As a consequence, the passive conductor presence further increases the multiconductor power flow size compared to the three-phase one. Therefore, the computational efficiency is fundamental to solve this problem in real networks.

In light of this, a multiconductor power flow method (PFPD_MCA), inspired by PFPD_3P, is developed and described in the following.

The power flow problem solution is computed by solving a set of equations based on some known technical constraints (usually positive sequence active/reactive power and voltage magnitudes). Typically, all the multiconductor grid busbars are grouped into three different categories: the slack busbar, the generator busbars, and the load busbars. At the three active conductors of each busbar, the following technical constraints are imposed:

1. For the ***SLACK busbar***: the positive sequence voltage $\underline{u}_{a,P}$ is set, both in magnitude and in angle. This voltage phasor represents the angle reference for all the network quantities;
2. For the ***Generator busbars***: the positive sequence voltage magnitude $\left|\underline{u}_{b,P}\right| \ldots \left|\underline{u}_{g,P}\right|$ and the injected positive sequence active power $p_{b,P} \ldots p_{g,P}$ are imposed;
3. For the ***Load busbars***: the absorbed positive sequence complex power $p_{h,P} + jq_{h,P} \ldots p_{m,P} + jq_{m,P}$ are constrained. The complex power is absorbed when the loads are subjected to their positive sequence nominal voltage. Instead, if the load is unbalanced, it is possible to constrain the three complex power absorbed by the active conductors.

The constraint elements admittances are stored into the multiconductor admittance matrix $\underline{\boldsymbol{Y}}_{\boldsymbol{SGL}}^{\boldsymbol{ABCM}}$; this matrix is a block diagonal square matrix. Since the busbars have not a number of passive conductors fixed *a priori*, but the number depends on the electrical elements connected to the busbar, the $\underline{\boldsymbol{Y}}_{\boldsymbol{SGL}}^{\boldsymbol{ABCM}}$ size is not strictly correlated to the number of busbars.

By knowing the multiconductor matrix $\underline{\boldsymbol{Y}}_{\boldsymbol{SGL}}^{\boldsymbol{ABCM}}$ and the multiconductor phase-to-ground voltage vector $\underline{\boldsymbol{u}}^{\boldsymbol{ABCM}}$, the following equation can be written:

$$\underline{\boldsymbol{i}}_{\boldsymbol{S}}^{\boldsymbol{ABCM}} = \underline{\boldsymbol{Y}}_{\boldsymbol{SGL}}^{\boldsymbol{ABCM}} \underline{\boldsymbol{u}}^{\boldsymbol{ABCM}} \tag{1}$$

where $\underline{\boldsymbol{i}}_{\boldsymbol{S}}^{\boldsymbol{ABCM}}$ is the block vector of the currents entering the multiconductor busbars of the constrained elements. In a busbar where no load is installed (*i.e.,* transit busbars) the corresponding elements of the matrix $\underline{\boldsymbol{Y}}_{\boldsymbol{SGL}}^{\boldsymbol{ABCM}}$ are null. Due to the possibility of considering the slack generator as a quasi-ideal current generator [32], also its admittance is stored inside $\underline{\boldsymbol{Y}}_{\boldsymbol{SGL}}^{\boldsymbol{ABCM}}$.

The multiconductor network admittance matrix $\underline{\boldsymbol{Y}}_{\boldsymbol{N}}^{\boldsymbol{ABCM}}$ correlates the multiconductor phase-to-ground voltages $\underline{\boldsymbol{u}}^{\boldsymbol{ABCM}}$ (expressed in (1)) with the currents entering the network $\underline{\boldsymbol{i}}_{\boldsymbol{N}}^{\boldsymbol{ABCM}}$:

$$\underline{\boldsymbol{i}}_{\boldsymbol{N}}^{\boldsymbol{ABCM}} = \underline{\boldsymbol{Y}}_{\boldsymbol{N}}^{\boldsymbol{ABCM}} \underline{\boldsymbol{u}}^{\boldsymbol{ABCM}} \tag{2}$$

By combining (1) with (2) element by element, the following equation is obtained:

$$\underline{\boldsymbol{i}}^{\boldsymbol{ABCM}} = \underline{\boldsymbol{Y}}^{\boldsymbol{ABCM}} \underline{\boldsymbol{u}}^{\boldsymbol{ABCM}} \tag{3}$$

where $\underline{\boldsymbol{Y}}^{\boldsymbol{ABCM}}$ is the multiconductor ''all-inclusive'' admittance matrix. This matrix holds all the power system information. The elements of the injected current vector $\underline{\boldsymbol{i}}^{\boldsymbol{ABCM}}$ are all zero except for the slack generator busbar. The current sub-vector of the slack generator terminals is equal to $\underline{\boldsymbol{J}}_{\boldsymbol{a}}^{\boldsymbol{ABCM}}$, since it corresponds to the multiconductor external current injection consequent to the current source representation of the slack generator at the positive sequence. As previously developed in [17] and [32], by exploiting (3), it is possible to develop a sequence of algebraic equations representing the

steady-state regime of the multiconductor network. By partitioning (3) in two sets of linear equations on the basis of the constraint typology, the following relations can be written:

$$\underline{\boldsymbol{i}}_{\boldsymbol{G}}^{\boldsymbol{ABCM}} = \underline{\boldsymbol{Y}}_{\boldsymbol{GG}}^{\boldsymbol{ABCM}} \underline{\boldsymbol{u}}_{\boldsymbol{G}}^{\boldsymbol{ABCM}} + \underline{\boldsymbol{Y}}_{\boldsymbol{GL}}^{\boldsymbol{ABCM}} \underline{\boldsymbol{u}}_{\boldsymbol{L}}^{\boldsymbol{ABCM}} \tag{4}$$

$$0^{\boldsymbol{ABCM}} = \underline{\boldsymbol{Y}}_{\boldsymbol{LG}}^{\boldsymbol{ABCM}} \underline{\boldsymbol{u}}_{\boldsymbol{G}}^{\boldsymbol{ABCM}} + \underline{\boldsymbol{Y}}_{\boldsymbol{LL}}^{\boldsymbol{ABCM}} \underline{\boldsymbol{u}}_{\boldsymbol{L}}^{\boldsymbol{ABCM}}. \tag{5}$$

By combining (4) with (5), (6) can be obtained:

$$\begin{aligned} \underline{\boldsymbol{i}}_{\boldsymbol{G}}^{\boldsymbol{ABCM}} &= \left[\underline{\boldsymbol{Y}}_{\boldsymbol{GG}}^{\boldsymbol{ABCM}} - \underline{\boldsymbol{Y}}_{\boldsymbol{GL}}^{\boldsymbol{ABCM}} \left(\underline{\boldsymbol{Y}}_{\boldsymbol{LL}}^{\boldsymbol{ABCM}} \right)^{-1} \underline{\boldsymbol{Y}}_{\boldsymbol{LG}}^{\boldsymbol{ABCM}} \right] \underline{\boldsymbol{u}}_{\boldsymbol{G}}^{\boldsymbol{ABCM}} \\ &= \underline{\boldsymbol{Y}}_{\boldsymbol{Geq}}^{\boldsymbol{ABCM}} \underline{\boldsymbol{u}}_{\boldsymbol{G}}^{\boldsymbol{ABCM}}. \end{aligned} \tag{6}$$

The matrix $\underline{\boldsymbol{Y}}_{\boldsymbol{Geq}}^{\boldsymbol{ABCM}}$ is the equivalent network as seen from the generator busbars. By applying matrix inversion to (6), it follows:

$$\underline{\boldsymbol{u}}_{\boldsymbol{G}}^{\boldsymbol{ABCM}} = \underline{\boldsymbol{Z}}_{\boldsymbol{Geq}}^{\boldsymbol{ABCM}} \underline{\boldsymbol{i}}_{\boldsymbol{G}}^{\boldsymbol{ABCM}}. \tag{7}$$

The current sub-vector at the slack generator busbar $\underline{\boldsymbol{J}}_{\boldsymbol{a}}^{\boldsymbol{ABCM}}$ can be computed from the inverse matrix $\underline{\boldsymbol{Y}}_{\boldsymbol{Geq,aa}}^{\boldsymbol{ABCM}}$ of the first block diagonal matrix of $\underline{\boldsymbol{Z}}_{\boldsymbol{Geq}}^{\boldsymbol{ABCM}}$ and the voltage sub-vector $\underline{\boldsymbol{u}}_{\boldsymbol{a}}^{\boldsymbol{ABCM}}$, *i.e.*,

$$\underline{\boldsymbol{J}}_{\boldsymbol{a}}^{\boldsymbol{ABCM}} = \underline{\boldsymbol{Y}}_{\boldsymbol{Geq,aa}}^{\boldsymbol{ABCM}} \underline{\boldsymbol{u}}_{\boldsymbol{a}}^{\boldsymbol{ABCM}}. \tag{8}$$

A. MODELLING OF THE CONSTRAINED BUSBARS

The $\underline{\boldsymbol{Y}}_{\boldsymbol{SGL}}^{\boldsymbol{ABCM}}$ matrix stores all the constrained element admittances: slack generator, generators and loads.

In the present algorithm, the slack generator is represented as a quasi-ideal current source. This approach is based on the formal possibility to perform a source transformation by considering the impedance of the voltage source generator exciting the network as a small value impedance (*i.e.*, $j10^{-6}$ p.u.). Therefore, the slack generator positive sequence network can be modelled as an ideal current generator in parallel with a very large value shunt admittance (*i.e.*, $-j10^{6}$ p.u.). The negative and zero sequence passive networks are fundamental to assess the impact of the slack generator on the voltage distortion. Hence, the slack generator admittance matrix at the sequence component $\underline{\boldsymbol{Y}}_{\boldsymbol{a}}^{\boldsymbol{0\,PN}}$ can be modelled. The corresponding phase matrix $\underline{\boldsymbol{Y}}_{\boldsymbol{a}}^{\boldsymbol{ABC}}$ can be determined by exploiting the Fortescue transformation. This matrix can be positioned in the multiconductor admittance matrix $\underline{\boldsymbol{Y}}_{\boldsymbol{SGL}}^{\boldsymbol{ABCM}}$.

Usually, in power generation busbars, synchronous generators are installed. These machines can be considered as a symmetrical device from a structural point of view. Thus, their steady-state regime can be studied by means of sequence networks. Since inverter-based power plants are always more present in the networks, the sequence component approach can be adopted also for these devices. The positive sequence network is the only active one since the power conversion occurs in this network. Nevertheless, in order to evaluate the generator effects on the unbalanced power flows, also the negative and the zero sequence admittances must be considered. The positive sequence admittance of the generator connected to the busbar g can be evaluated as in the following:

$$\underline{y}_{g,P} = -\frac{p_{g,P}}{\left|\underline{u}_{g,P}\right|^2} + j\frac{q_{g,P}}{\left|\underline{u}_{g,P}\right|^2}. \tag{9}$$

Hence, the diagonal admittance matrix at the sequence component $\underline{\boldsymbol{Y}}_{\boldsymbol{g}}^{\boldsymbol{0\,PN}}$ can be modelled. The phase matrix $\underline{\boldsymbol{Y}}_{\boldsymbol{g}}^{\boldsymbol{ABC}}$ can be determined by exploiting the Fortescue transformation.

This matrix can be positioned at the active terminals of the busbar g of the multiconductor admittance matrix $\underline{\boldsymbol{Y}}_{\boldsymbol{SGL}}^{\boldsymbol{ABCM}}$.

For the load busbars, if a balanced load is connected to the busbar l, this can be easily modelled by exploiting the sequence frame of reference approach. This load can be thought as a composition of two different load typologies: the asynchronous load **(1)** and the static load **(2)**. These load types can be considered in parallel with each other without mutual coupling. By denoting with $\underline{s}_{t,P}$ the positive sequence complex power absorbed by each of the two load typologies under the positive sequence nominal voltage (*i.e.*, 1 *p.u.*), the positive sequence admittance can be computed with the following relation:

$$\underline{y}_{t,P} = \frac{\underline{S}_{t,P}^{*}}{\left|\underline{u}_{t,P}\right|^2} = \frac{p_{t,P} - jq_{t,P}}{1^2}, \quad t = 1, 2 \tag{10}$$

where $p_{l,P}$ and $q_{l,P}$ are the positive sequence active and reactive power. For the static load, the positive and negative sequences are equal. Instead, for the asynchronous load the negative sequence admittance can be considered equal to $\xi \underline{y}_{P,1} e^{j\psi}$, where $\xi = 5 \div 7$ and $\psi = -60° \div -75°$ [33]. Thus, the diagonal admittance matrix at the sequence component $\underline{\boldsymbol{Y}}_{\boldsymbol{l}}^{\boldsymbol{0PN}}$ can be assembled by summing together the sequence admittance matrix of the two load typologies:

$$\underline{\boldsymbol{Y}}_{\boldsymbol{l}}^{\boldsymbol{0\,PN}} = \underline{\boldsymbol{Y}}_{\boldsymbol{l,1}}^{\boldsymbol{0\,PN}} + \underline{\boldsymbol{Y}}_{\boldsymbol{l,2}}^{\boldsymbol{0\,PN}} \tag{11}$$

Eventually, the phase matrix $\underline{\boldsymbol{Y}}_{\boldsymbol{l}}^{\boldsymbol{ABC}}$ can be determined by exploiting Fortescue transformation. This matrix can be positioned in the active terminals of the busbar l of the multiconductor admittance matrix $\underline{\boldsymbol{Y}}_{\boldsymbol{SGL}}^{\boldsymbol{ABCM}}$.

When performing an unbalanced power flow, also the unbalanced loads must be taken into account. In this case, the complex power absorbed by each of the three phases $\underline{s}_A$, $\underline{s}_B$, $\underline{s}_C$ must be specified. Unfortunately, the sequence frame of reference approach cannot be exploited. The unbalanced load is star connected. Thus, the phase component matrix $\underline{\boldsymbol{Y}}_{\boldsymbol{l}}^{\boldsymbol{ABC}}$ can be computed (see Fig. 1) and added to the multiconductor admittance matrix $\underline{\boldsymbol{Y}}_{\boldsymbol{SGL}}^{\boldsymbol{ABCM}}$.

B. NETWORK ELEMENTS MODELLING

The $\underline{\boldsymbol{Y}}_{\boldsymbol{N}}^{\boldsymbol{ABCM}}$ matrix stores all the network element admittances: lines, transformers, and capacitive/inductive shunt elements.

The transmission lines are modelled by considering all the conductors, both active and passive ones (*i.e.*, OHL ground wires, IC metallic screens/armours and GIL enclosures). In order to consider n parallel conductors, a multiconductor

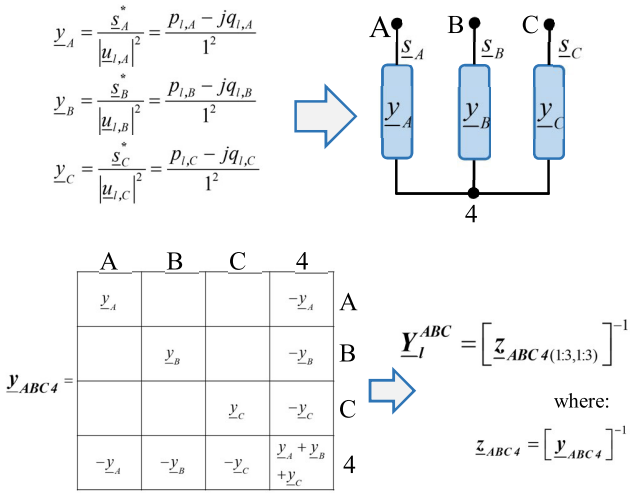

FIGURE 1. Representation of the three-phase unbalanced load.

approach is adopted [29]. The approach, developed by the first author in 2009, is known with the acronym MCA.

In this method, the lines are represented as a cascade of elementary cells of length Δ (suitably chosen, *i.e.*, span length for OHLs, in the range between 10 and 100 m for ICs) modelled by a lumped π-circuit.

Being Δ sufficiently small, the uniformly distributed shunt admittances can be lumped at both ends of the cell (transverse blocks $\underline{\boldsymbol{Y}}_{\boldsymbol{ssT}}$ and $\underline{\boldsymbol{Y}}_{\boldsymbol{rrT}}$) and the longitudinal elements can be considered separately in the block $\underline{\boldsymbol{Y}}_{\boldsymbol{L}}$. In Fig. 2 the multiconductor elementary cell is shown. At power frequency (50-60 Hz), self and mutual longitudinal impedances can be evaluated by means of any of these theories: Schelkunoff/Pollaczek - Carson/Clem – Carson - Wedepohl. By combining $\underline{\boldsymbol{Y}}_{\boldsymbol{ssT}}$, $\underline{\boldsymbol{Y}}_{\boldsymbol{rrT}}$ and $\underline{\boldsymbol{Y}}_{\boldsymbol{L}}$, the matrix formulation linking the currents entering into elementary cell ends $\underline{\boldsymbol{i}}_{\Delta}$ with their voltages $\underline{\boldsymbol{u}}_{\Delta}$ can be obtained:

$$\underbrace{\begin{bmatrix}\underline{\boldsymbol{i}}_s\\ \underline{\boldsymbol{i}}_r\end{bmatrix}}_{\underline{\boldsymbol{i}}_{\Delta}} = \underbrace{\left[\begin{bmatrix}\underline{\boldsymbol{Y}}_{ss1} & \\ & \underline{\boldsymbol{Y}}_{rr1}\end{bmatrix} + \underline{\boldsymbol{Y}}_{\boldsymbol{L}}\right]}_{\underline{\boldsymbol{Y}}_{\Delta}} \underbrace{\begin{bmatrix}\underline{\boldsymbol{u}}_s\\ \underline{\boldsymbol{u}}_r\end{bmatrix}}_{\underline{\boldsymbol{u}}_{\Delta}} \tag{12}$$

Hence, the cascade of the elementary cell matrices is performed in order to compute the admittance matrix of the entire line. Fig. 3 shows the formulation for the cascade of two elementary cells, this process is repeated for the entire line length. Thus, a unique admittance matrix representing the entire line as seen from its busbars can be evaluated.

The MCA approach allows modelling the different elements of the lines, *e.g.*, cross-bonding boxes. All these elements are considered by means of suitable admittance matrices and positioned in the corresponding cell. The steady-state regime of power transformers, both two and three windings, can be modelled by means of symmetrical

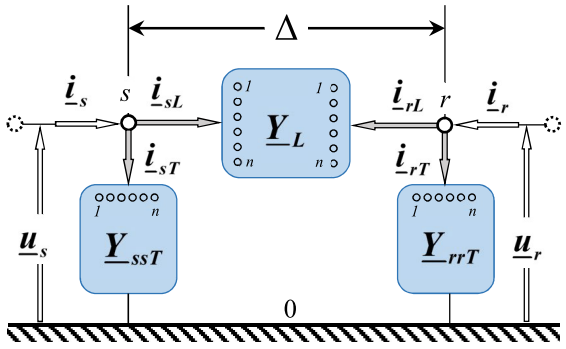

FIGURE 2. Multiconductor elementary cell.

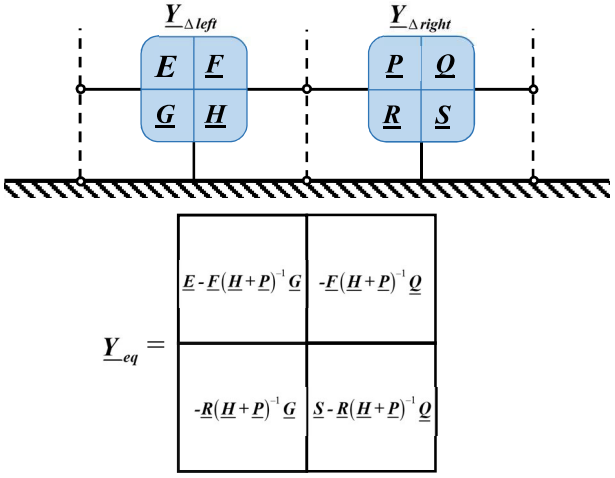

FIGURE 3. Matrix procedure to calculate the cascade of two elementary cells.

component approach, since these devices can be considered symmetrical from a structural point of view. For two winding transformers, the sequence networks are immediately inferable from the nameplate data and the winding earthing impedances.

For each one of these networks, the corresponding (2×2) admittance matrix is assembled, and the admittance sequence matrix (6×6) $\underline{\boldsymbol{Y}}_{\boldsymbol{2w-tr}}^{\boldsymbol{0PN}}$ is computed by means of the incidence matrix. Eventually, the phase matrix $\underline{\boldsymbol{Y}}_{\boldsymbol{2w-tr}}^{\boldsymbol{ABC}}$ is determined by exploiting the generalized Fortescue transformation [33].

The present procedure can be extended to the three-winding transformers. For a three-winding transformer, the dimension of the sequence network admittance matrix is (3×3). The three admittance matrices are assembled in a unique (9×9) admittance sequence matrix $\underline{\boldsymbol{Y}}_{\boldsymbol{3w-tr}}^{\boldsymbol{0PN}}$, and the phase matrix $\underline{\boldsymbol{Y}}_{\boldsymbol{3w-tr}}^{\boldsymbol{ABC}}$ is determined by means of the generalized Fortescue transformation.

The network matrix $\underline{\boldsymbol{Y}}_{\boldsymbol{N}}^{\boldsymbol{ABCM}}$ also holds the shunt elements, *i.e.*, capacitive/inductive reactive compensation, inductive reactive compensation of land/submarine ICs. The corresponding admittance matrix can be computed and positioned in the suitable busbar of the multiconductor network matrix $\underline{\boldsymbol{Y}}_{\boldsymbol{N}}^{\boldsymbol{ABCM}}$.

C. ITERATIVE PROCEDURE

The presented iterative procedure does not exploit any numerical analysis technique, but it is based on a matrix method. The initial values of the constrained element admittances stored in the multiconductor matrix $\underline{\boldsymbol{Y}}_{\boldsymbol{SGL}}^{\boldsymbol{ABCM}}$ can be set equal to:

1) FOR THE SLACK-GENERATOR

$$\underline{y}_{a,P} = -j \cdot 10^5 \text{p.u.}$$

As previously mentioned, the slack generator is modelled as a quasi-ideal current source in the positive sequence network. The discussion about the $\underline{y}_{a,P}$ magnitude is analogous to the one presented in [32]. For the negative and zero sequence networks, the admittances of the synchronous machine chosen as slack generator are considered. Hence, the slack generator admittance matrix at the sequence component $\underline{\boldsymbol{Y}}_{\boldsymbol{a}}^{\boldsymbol{0\,PN}}$ is assembled. By exploiting the Fortescue transformation, the corresponding phase matrix is computed, and then it is stored inside $\underline{\boldsymbol{Y}}_{\boldsymbol{SGL}}^{\boldsymbol{ABCM}}$ in the suitable position.

2) FOR THE LOAD BUSBARS

The phase admittance matrix $\underline{\boldsymbol{Y}}_{\boldsymbol{l}}^{\boldsymbol{ABC}}$ in each load busbar is computed by considering its nominal positive sequence voltage magnitude, *i.e.*, 1 p.u. Then, it is stored in the corresponding position of $\underline{\boldsymbol{Y}}_{\boldsymbol{SGL}}^{\boldsymbol{ABCM}}$. In order to assess the voltage distortion in the entire network, also the negative and zero sequence admittances of load busbars are modelled.

3) FOR THE GENERATOR BUSBARS

In these busbars, only the positive sequence network is the active one. In fact, the constrained quantities are the positive sequence voltage magnitude $\left|\underline{u}_{b,P}\right| \ldots \left|\underline{u}_{g,P}\right|$ and the injected positive sequence active power $p_{b,P} \ldots p_{g,P}$. By means of (9), the positive sequence admittance of the generator in busbar g is computed:

$$\underline{y}_{g,P} = -\frac{p_{g,P}}{\left|\underline{u}_{g,P}\right|^2} + j\frac{q_{g,P}}{\left|\underline{u}_{g,P}\right|^2} \tag{13}$$

the admittance of (13) is the initial guess of the iterative procedure. Analogously to the transformers, the negative and the zero sequence admittances are immediately inferable from the nameplate data and the winding earthing impedance.

In (13), the only unconstrained quantity is the injected reactive power $q_{g,P}$. Also for PDPF_MCA, a good reactive power initial guess is needed to start the iterative method [34] and to perform a fast power flow convergence, as demonstrated in [32]. Thus, all the generator positive sequence reactive powers $q_{b,P} \div q_{g,P}$ must be estimated. As in [17] and [32], the multiconductor network matrix $\underline{\boldsymbol{Y}}_{\boldsymbol{N}}^{\boldsymbol{ABCM}}$ is considered as ideal (both the longitudinal resistances and the transversal conductances are neglected) and in the matrix $\underline{\boldsymbol{Y}}_{\boldsymbol{SGL}}^{\boldsymbol{ABCM}}$ only the load nominal admittances are considered. By combining $\underline{\boldsymbol{Y}}_{\boldsymbol{N}}^{\boldsymbol{ABCM}}$ with $\underline{\boldsymbol{Y}}_{\boldsymbol{SGL}}^{\boldsymbol{ABCM}}$, the multiconductor "all-inclusive" admittance matrix $\underline{\boldsymbol{Y}}^{\boldsymbol{ABCM}}$ is obtained. The voltage phasors at generator busbars have magnitude equal to the constrained ones and zero angle.

Eq. (6) is applied, and the currents injected at the generator busbars $\underline{\boldsymbol{i}}_{\boldsymbol{G}}^{\boldsymbol{ABCM}}$ are computed. Then, the Fortescue transformation is exploited to compute the symmetrical components of the active conductor electrical quantities. Hence, the positive sequence reactive powers injected in the generator busbars $q_{b,P} \div q_{g,P}$ are obtained.

The iterative algorithm is based on the injection of correcting current vectors into the generation $\underline{\Delta \boldsymbol{i}}_{\boldsymbol{G}}^{\boldsymbol{ABCM}}$ and the load $\underline{\Delta \boldsymbol{i}}_{\boldsymbol{L}}^{\boldsymbol{ABCM}}$ busbars. It is the multiconductor generalization of the procedure presented in [17]. In order to assess the power flow solution, (14)÷(18) are iteratively applied until convergence is reached, *i.e.*, until any mismatch of generator positive sequence voltage magnitude is within the tolerance.

Equations (14)÷(18) are referred to the k-th iteration:

$$\underline{\boldsymbol{u}}_{\boldsymbol{G}}^{\boldsymbol{ABCM}} = \underline{\boldsymbol{Z}}_{\boldsymbol{Geq}}^{\boldsymbol{ABCM}} \left[\underline{\Delta \boldsymbol{i}}_{\boldsymbol{G,c\_q}}^{\boldsymbol{ABCM}} - \underline{\boldsymbol{Y}}_{\boldsymbol{GL}}^{\boldsymbol{ABCM}} \left(\underline{\boldsymbol{Y}}_{\boldsymbol{LL}}^{\boldsymbol{ABCM}} \right)^{-1} \underline{\Delta \boldsymbol{i}}_{\boldsymbol{L,c}}^{\boldsymbol{ABCM}} \right] \tag{14}$$

$$\underline{\boldsymbol{u}}_{\boldsymbol{L,c}}^{\boldsymbol{ABCM}} = -\left(\underline{\boldsymbol{Y}}_{\boldsymbol{LL}}^{\boldsymbol{ABCM}} \right)^{-1} \left[\underline{\boldsymbol{Y}}_{\boldsymbol{LG}}^{\boldsymbol{ABCM}} \underline{\boldsymbol{u}}_{\boldsymbol{G}}^{\boldsymbol{ABCM}} + \underline{\Delta \boldsymbol{i}}_{\boldsymbol{L,c}}^{\boldsymbol{ABCM}} \right] \tag{15}$$

$$\underline{\Delta \boldsymbol{i}}_{\boldsymbol{L,c}}^{\boldsymbol{0\,PN}} = -\underline{\boldsymbol{Y}}_{\boldsymbol{L,P}} \odot \left(1 - \left| \underline{\boldsymbol{u}}_{\boldsymbol{L,c,P}} \right|^2 \right) \Big/ \left(\underline{\boldsymbol{u}}_{\boldsymbol{L,c,P}} \right)^* \tag{16}$$

$$\underline{\Delta \boldsymbol{i}}_{\boldsymbol{G,c}}^{\boldsymbol{ABCM}} = \underline{\boldsymbol{Y}}_{\boldsymbol{Geq}}^{\boldsymbol{ABCM}} \underline{\boldsymbol{u}}_{\boldsymbol{G,c}}^{\boldsymbol{ABCM}} + \underline{\boldsymbol{Y}}_{\boldsymbol{GL}}^{\boldsymbol{ABCM}} \left(\underline{\boldsymbol{Y}}_{\boldsymbol{LL}}^{\boldsymbol{ABCM}} \right)^{-1} \underline{\Delta \boldsymbol{i}}_{\boldsymbol{L,c}}^{\boldsymbol{ABCM}} \tag{17}$$

$$\underline{\Delta \boldsymbol{i}}_{\boldsymbol{G,c\_q,P}} = -j \left[Im \left(\underline{\boldsymbol{u}}_{\boldsymbol{G,c,P}} \otimes \underline{\Delta \boldsymbol{i}}_{\boldsymbol{G,c,P}}^* \right) \right] \Big/ \underline{\boldsymbol{u}}_{\boldsymbol{G,c,P}}^* \tag{18}$$

For the slack busbar, (18) must not be applied (since both the positive sequence active and reactive power are unknown quantities), it follows:

$$\underline{\Delta \boldsymbol{i}}_{\boldsymbol{G,c\_q,P}}(1,1) = \underline{\Delta \boldsymbol{i}}_{\boldsymbol{G,c,P}}(1,1)$$

Equations (14), (15) and (17) are the generalization of (4) and (5), once the correcting current vectors into the generation $\underline{\Delta \boldsymbol{i}}_{\boldsymbol{G}}^{\boldsymbol{ABCM}}$ and the load $\underline{\Delta \boldsymbol{i}}_{\boldsymbol{L}}^{\boldsymbol{ABCM}}$ busbars are considered. Since the power conversion takes place in the positive sequence network, the correcting currents of (16) and (18) are computed in this network. These formulae are developed starting from the busbar constraints (*i.e.*, positive sequence active power and voltage magnitude for the generator busbars, positive sequence complex power for the load busbars). Equation (18) evaluates the positive sequence quadrature component current vector that injects the same value of positive sequence reactive power of (17).

In (16), the symbol "⊙" is adopted as "positive sequence multiplication". This symbol is exploited to synthetize the procedure giving the sequence correcting current due to the positive sequence voltage $\underline{\boldsymbol{u}}_{\boldsymbol{L,c,P}}$ only, since the power conversion takes place in this sequence. Hence, $\underline{\boldsymbol{u}}_{\boldsymbol{L,c,P}}$ and the elements correlated to the positive sequence voltage of the load admittance submatrix $\underline{\boldsymbol{Y}}_{\boldsymbol{L}}^{\boldsymbol{0\,PN}}$ must be considered in (16). All the elements connected to the positive sequence voltage of $\underline{\boldsymbol{Y}}_{\boldsymbol{L}}^{\boldsymbol{0\,PN}}$ are stored in the matrix $\underline{\boldsymbol{Y}}_{\boldsymbol{L,P}}$. This

approach can be applied both for balanced and unbalanced loads.

Before these correcting currents are applied into (14), (15) and (17), they must be converted in the phase frame of reference. The Fortescue transformations consider only the active conductors, in order to apply the transformation an incidence matrix $\boldsymbol{R}$ is exploited both to exclude and to reintroduce the passive conductor electrical quantities.

Fig. 4 shows the flow-chart of PFPD_MCA. In the first iteration (i.e., $k = 0$), the correcting current vectors, both generator and load, are all set to zero except for the slack busbar. After calculating $\underline{\boldsymbol{u}}_{\boldsymbol{G}}^{\boldsymbol{ABCM}}$ by means of (14), the Fortescue transformation computes the generator voltages in the sequence frame of reference. The incidence matrix $\boldsymbol{R}$ is exploited to remove passive conductor voltages before Fortescue transformation is applied. Thus, the matrix $\underline{\boldsymbol{T}}_{\boldsymbol{x}}$ corrects the positive sequence voltage magnitude of all the generator busbars, these voltage magnitudes are imposed equal to the constraint positive sequence voltages $|\underline{u}_{a,P}| \dots |\underline{u}_{g,P}|$, instead, the voltage angles $\delta_b \cdots \delta_g$ are kept the same.

Then, the inverse Fortescue transformation allows returning to the phase frame of reference, the passive conductor voltages are reintroduced by exploiting the matrix $\boldsymbol{R}^{\mathrm{T}}$. Eq. (15) computes the multiconductor phase voltages of the load busbars $\underline{\boldsymbol{u}}_{\boldsymbol{L,c}}^{\boldsymbol{ABCM}}$. Equations (14) and (15) allow assessing the voltages in all the grid busbars, these voltages are necessary to compute the correcting current vectors.

III. SUBSTATION PASSIVE CONDUCTOR MODELLING

In order to evaluate the multiconductor power flow, the presence of passive conductors must be considered. This section focuses on the multiconductor network admittance matrix building. In PFPD_MCA, all the different passive conductors can be modelled, *e.g.*, ground wires of OHLs or screens of ICs.

In each network busbar, a generic number n of conductors can be connected: the first three conductors represent the active ones and the following are the passive ones. As abovementioned in Sect. II, each network busbar has not a number of passive conductors fixed *a priori*, but the number depends on the electrical elements connected to it.

In the multiconductor network admittance matrix, the number of rows and columns is assigned depending on the *maximum number of conductors* connected to the busbar. For instance, let us suppose that an OHL with a unique ground wire (for this line, the number of conductors is *4*, *i.e.*, *3* active conductors and *1* ground wire) and an IC line with cross-bonding arrangement (in this case, the number of conductors is *6*, *i.e.*, *3* active conductors and *3* metallic screens) converge on the same busbar. For this busbar, the number of terminals is assigned equal to *6*. This operation must be repeated for all the network busbars before the multiconductor network admittance matrix is built.

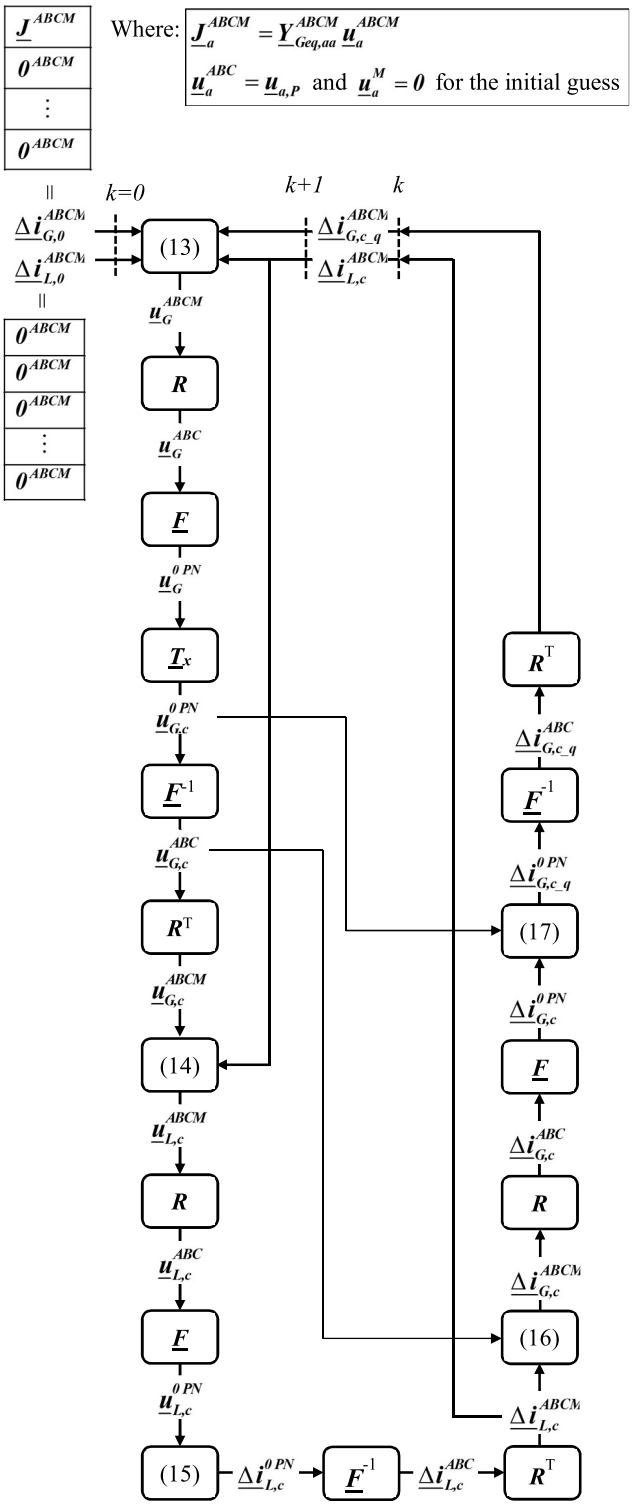

FIGURE 4. Flow chart of the PFPD_MCA algorithm.

When electrical lines with a different conductor number converge on a busbar, the first three conductors, *i.e.,* the active ones, are connected to the first *3* busbar terminals and the following conductors, *i.e.,* the passive ones, are connected

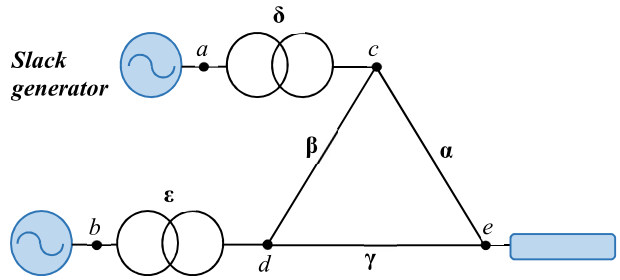

FIGURE 5. Elementary system with five busbars, five branch elements and three shunt elements.

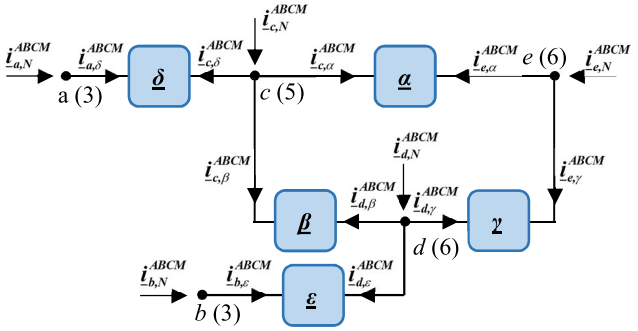

FIGURE 6. Schematic representation of the elementary network of Fig. 5. The generators and the loads are excluded. The number inside the round brackets indicates the number of terminals of each busbar.

to the following terminals starting from the 4^{th} terminal. In order to automatically implement the formation of the multiconductor network matrix $\underline{\boldsymbol{Y}}_{\boldsymbol{N}}^{\boldsymbol{ABCM}}$, a primitive matrix $\underline{\boldsymbol{Y}}_{\boldsymbol{P}}^{\boldsymbol{ABCM}}$ and an incidence matrix $\boldsymbol{S}$ are exploited.

For the grid represented in Fig. 5, (where $\boldsymbol{\alpha}$ is an OHL with a single ground wire, $\boldsymbol{\beta}$ is an OHL with two ground wires and $\boldsymbol{\gamma}$ is an underground IC) the diagram of Fig. 6 can be built (generators and loads are omitted).

In this diagram $\underline{\boldsymbol{\alpha}}$ (8×8), $\underline{\boldsymbol{\beta}}$ (10×10), $\underline{\boldsymbol{\gamma}}$ (12×12), $\underline{\boldsymbol{\delta}}$ (6×6), $\underline{\boldsymbol{\varepsilon}}$ (6×6) are the admittance matrices of the network elements and $\underline{\boldsymbol{i}}_{\boldsymbol{c,\alpha}}^{\boldsymbol{ABCM}} \div \underline{\boldsymbol{i}}_{\boldsymbol{d,\varepsilon}}^{\boldsymbol{ABCM}}$ are the currents entering into their terminals. Furthermore, according to the previous assumption, the number of terminals of each busbar is reported in Fig. 6.

Fig. 7 shows the matrix relation between currents and voltages at the two ends of each component. So, a unique matrix formulation between nodal voltages and entering currents can be written:

$$\underline{\boldsymbol{i}}_{\boldsymbol{P}}^{\boldsymbol{ABCM}} = \underline{\boldsymbol{Y}}_{\boldsymbol{P}}^{\boldsymbol{ABCM}} \underline{\boldsymbol{u}}_{\boldsymbol{P}}^{\boldsymbol{ABCM}} \tag{19}$$

where $\underline{\boldsymbol{Y}}_{\boldsymbol{P}}^{\boldsymbol{ABCM}}$ is a block diagonal matrix. The vector $\underline{\boldsymbol{u}}_{\boldsymbol{P}}^{\boldsymbol{ABCM}}$ is built from the combination of the incidence matrix $\boldsymbol{S}$ and the multiconductor phase-to-ground voltage vector $\underline{\boldsymbol{u}}^{\boldsymbol{ABCM}}$, as reported in Fig. 8. The incident matrix $\boldsymbol{S}$ is formed by the composition of identity matrices $\boldsymbol{I}$, the size of each incidence matrix depends on the admittance matrix size of the corresponding line.

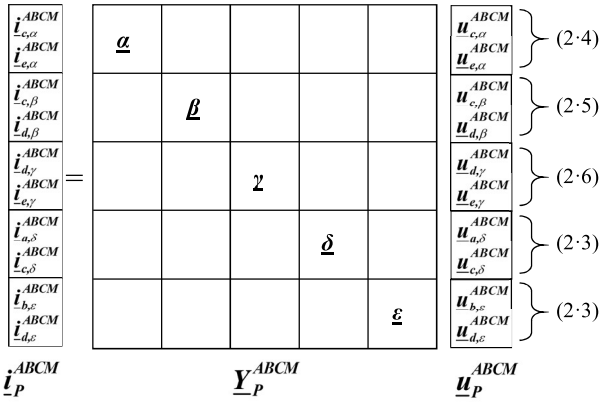

FIGURE 7. Primitive matrix representation of the network of Fig. 5.

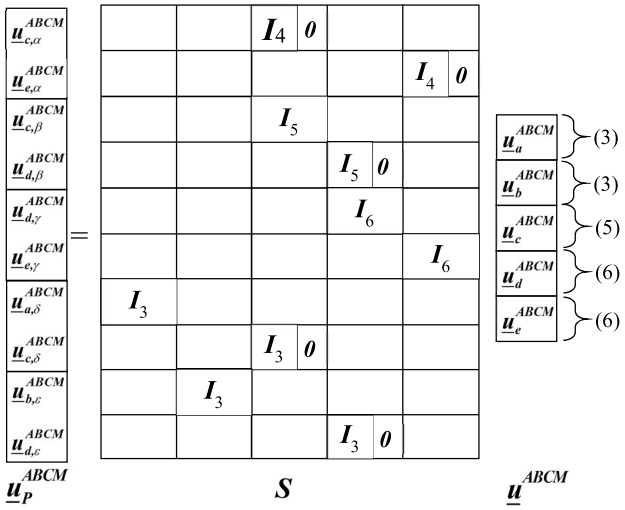

FIGURE 8. Matrix representation of (19) for the network of Fig. 5. The subscript in the identity matrices denotes the size.

In fact, the matrix multiplication of $\boldsymbol{S}$ and $\underline{\boldsymbol{u}}^{\boldsymbol{ABCM}}$ must produce a vector where the voltage sub-vectors have the same dimension of the corresponding line in $\underline{\boldsymbol{Y}}_{\boldsymbol{P}}^{\boldsymbol{ABCM}}$.

Since in each busbar, the number of terminals depends on the maximum number of conductors connected to the busbar, the size of each identity matrix $\boldsymbol{I}$ must be coherent with the corresponding line.

If the number of the conductors in a line is less than the terminals present in its own busbar, a null matrix is introduced to respect the size of the multiconductor phase-to-ground voltage vector $\underline{\boldsymbol{u}}^{\boldsymbol{ABCM}}$ sub-vectors.

$$\underline{\boldsymbol{u}}_{\boldsymbol{P}}^{\boldsymbol{ABCM}} = \boldsymbol{S}\underline{\boldsymbol{u}}^{\boldsymbol{ABCM}} \tag{20}$$

The vector $\underline{\boldsymbol{i}}_{\boldsymbol{N}}^{\boldsymbol{ABCM}}$ of the currents entering in to the network $\underline{\boldsymbol{i}}_{\boldsymbol{a,N}}^{\boldsymbol{ABCM}} \div \underline{\boldsymbol{i}}_{\boldsymbol{e,N}}^{\boldsymbol{ABCM}}$ can be computed as:

$$\underline{\boldsymbol{i}}_{\boldsymbol{N}}^{\boldsymbol{ABCM}} = \boldsymbol{S}^{T} \underline{\boldsymbol{i}}_{\boldsymbol{P}}^{\boldsymbol{ABCM}} \tag{21}$$

where $\boldsymbol{S}^{\mathrm{T}}$ is the transpose matrix of $\boldsymbol{S}$.

Fig. 9 represents the matrix relation of (21).

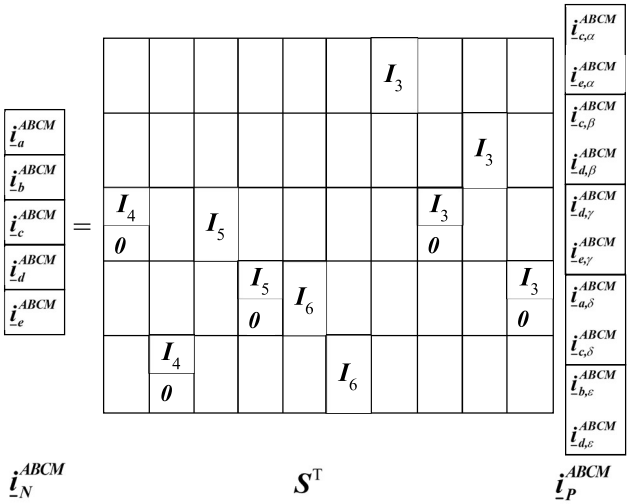

FIGURE 9. Matrix representation of (20) for the network of Fig. 5. The subscript in the identity matrices denotes the matrix size.

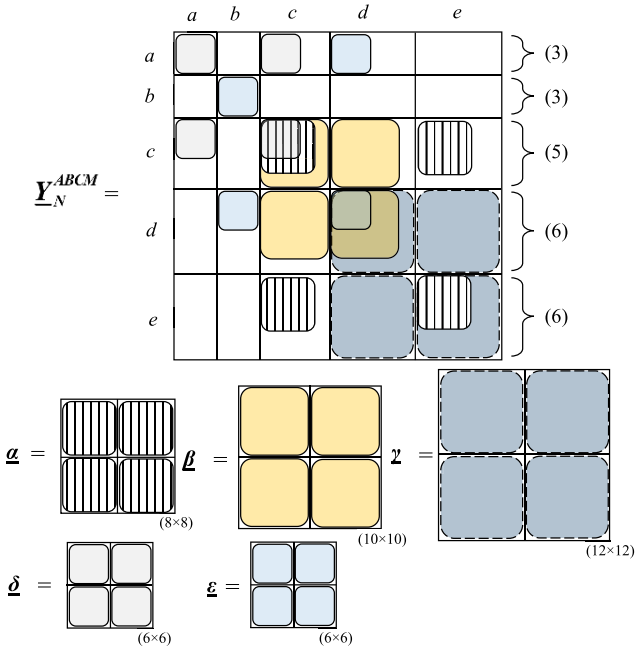

FIGURE 10. Matrix $\underline{\boldsymbol{Y}}_N^{ABCM}$ of the network of Fig. 5.

By combining (19) with (20) into (21), it yields:

$$\underline{\boldsymbol{i}}_N^{ABCM} = \boldsymbol{S}^T \underline{\boldsymbol{Y}}_P^{ABCM} \boldsymbol{S} \underline{\boldsymbol{u}}^{ABCM} \tag{22}$$

Therefore, by comparing (22) with (2), the multiconductor admittance matrix $\underline{\boldsymbol{Y}}_N^{ABCM}$ of the network is given by:

$$\underline{\boldsymbol{Y}}_N^{ABCM} = \boldsymbol{S}^T \underline{\boldsymbol{Y}}_P^{ABCM} \boldsymbol{S} \tag{23}$$

According to the grid of Fig. 5, $\underline{\boldsymbol{Y}}_N^{ABCM}$ is a block sparse matrix, where the coloured squares of Fig. 10 represent the admittance matrices of the branch elements.

In real power systems, different network busbars are located in the same electrical substation. For instance, the transformer windings are connected to two different busbars with different voltage levels. These busbars are positioned in the same electrical substation. In this case, it is fundamental to model the passive conductors in a suitable manner, since all the passive conductors of the same electrical substation busbars are connected to the substation grounding system, as shown in Fig. 11. Therefore, the passive conductor voltage phasor is the same in all the passive conductors of all the electrical substation busbars.

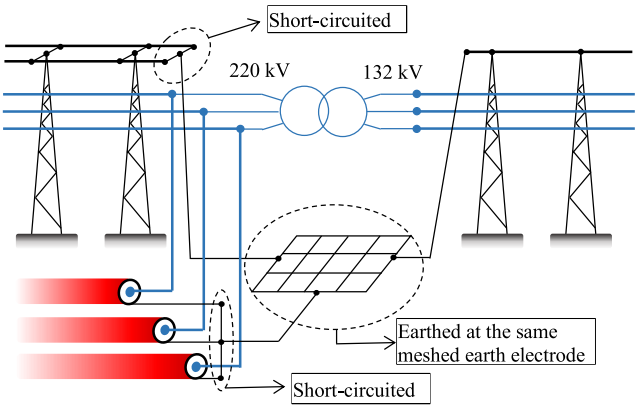

FIGURE 11. Substation passive conductor connections.

In order to model this configuration, two operations must be performed during the multiconductor admittance matrix $\underline{\boldsymbol{Y}}_N^{ABCM}$ building:

- The passive conductors of each busbar are connected by means of large conductances (*i.e.*, 10^6 p.u.). For example, when the IC screens reach a substation, they are short-circuited together and then they are earthed at the substation grounding system;
- The passive conductors of the network busbars located in the same electrical substation are jointed together by means of large conductances and linked to the substation grounding system.

In PFPD_MCA, each network busbar is assigned to the corresponding substation. The network substations are characterized by their own extension of the meshed earth electrode and soil resistivity. By exploiting IEC formula [35], the resistance to earth of the meshed earth electrode can be computed:

$$R_E = \frac{\rho_E}{2D} [\Omega] \tag{24}$$

where ρ_E is the substation soil resistivity [$\Omega\cdot$ m] and D is the diameter of a circle with the same area as the meshed earth electrode. Since all the elements of $\underline{\boldsymbol{Y}}_N^{ABCM}$ are in p.u., also the resistance to earth of the meshed earth electrode must be assessed in p.u. The *per unit* resistance to earth is positioned in the corresponding passive conductor element of $\underline{\boldsymbol{Y}}_N^{ABCM}$.

It is important to highlight that the *per unit* resistance to earth is assigned to an arbitrary busbar of the electrical substation. Then, in each busbar of the network, the passive conductor terminals are short-circuited together. Eventually, a short-circuit matrix is built between the first passive

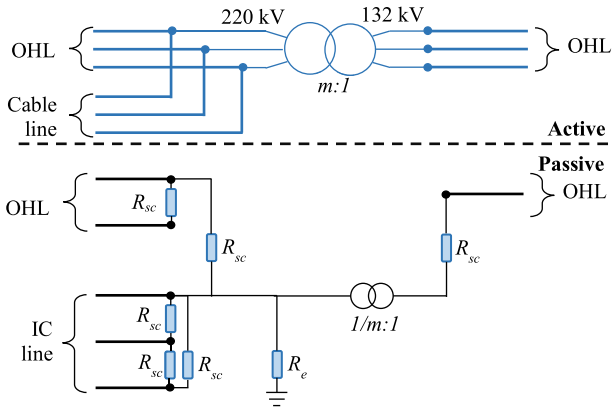

FIGURE 12. Circuital representation of active/passive conductor connections in electrical substations.

conductor of each busbar located in the same substation. In PFPD_MCA, the power flow is solved by means of *per unit* method, hence the line admittances are referred to their own nominal voltage. The passive conductors of different voltage busbars cannot be directly short-circuited together, since the corresponding p.u. line admittances are referred to different voltages.

In fact, in real power systems, all the passive conductor terminals belonging to the same electrical substation have the same absolute voltage value. In this power flow algorithm, the passive conductors of the busbars belonging to the same electrical substation could be referred to different base voltage. Hence, an ideal transformer must be installed between different voltage passive conductor terminals, as shown in Fig. 12. This ideal transformer has a turn ratio equal to the reciprocal of the base voltage ratio, since the higher voltage passive conductor terminals have a lower p.u. voltage and the lower voltage passive conductor terminals have a higher p.u. voltage. The single-phase ideal transformer is built by exploiting the transmission matrix and the admittance matrix, then it is positioned in the suitable elements of $\underline{\boldsymbol{Y}}_{\boldsymbol{N}}^{\boldsymbol{ABCM}}$.

IV. CASE STUDIES

In this section, the PFPD_MCA is applied to assess network power quality (limited to electrical quantity unbalances) and electromagnetic compatibility (limited to ground return current magnitude).

Two case studies are presented to show the algorithm effectiveness: an 18-busbar 380 kV transmission network and a 39-busbar network. In the second case study, different voltage levels are installed.

In order to confirm the validity of the PFPD_MCA results, the voltages in all the network busbars are compared with the corresponding ones evaluated in the equivalent single-phase circuit at the positive sequence and with the three-phase power-flow algorithm. The chosen equivalent single-phase power flow algorithm is PFPD [32]. Instead, the three-phase power flow is assessed by the commercial software DGS. This software englobes the passive conductor effects into the active conductors by means of Kron's matrix reduction technique. The differences between the positive sequence voltages calculated with PFPD_MCA and the equivalent single-phase circuit voltages computed with PFPD are assessed for angles and magnitudes. The commercial software results are compared in angle and magnitude for the three phases. Furthermore, to appreciate the computation power of PFPD_MCA, the electrical quantities along the lines are shown, both in active conductors and in passive ones.

The approach adopted to assess the electrical quantities along the lines is named *SPLIT*: it allows rebuilding the electrical quantity behaviours along a line starting from the voltages at the two ends.

The *SPLIT* method is deeply presented in App.

A. THE 18 SECTION NETWORK

The 18-section case study (see Fig. 13) consists of *3* generator buses and *15* load buses (some of these are transit sections, where the complex power is zero).

All the loads are three-phase symmetrical ones, this configuration represents the reality since the HV/EHV grids are operated with symmetrical loads.

The network busses are interconnected each other by means of *15* lines. Different line technologies are adopted: single and double-circuit OHLs, land single-core ICs and armoured submarine single-core ICs. For the land single-core ICs, different screen configurations are considered: the line between the busses 9 and 10 has a cross-bonding screen arrangement with *13* major sections, instead, the line between the busses 8 and 9 and between the busses 10 and 11 have a solid-bonding screen arrangement.

The armoured submarine single-core IC line interconnecting the nodes 16 and 17 has solid-bonded screens, the three screens are earthed to the armour wires every 5 km. The adopted IC structure is the same of the submarine link between Sicily and Italian peninsula [36]. With the aim of representing the cable link structure faithfully, shunt reactors are installed at the ends of the lines to compensate the reactive power absorption.

In the equivalent single-phase circuit studied with PFPD, the transmission lines are represented by considering their positive sequence per unit length parameters r, l, c, g. These electrical parameters do not include the passive conductor power loss effects: this approach causes a wrong evaluation of Joule losses in case of passive conductor current circulation, *e. g.*, solid-bonded ICs, cross-bonded ICs with different minor section lengths, armoured submarine ICs. Firstly, all the power flow solution differences between PFPD_MCA and PFPD are assessed, and maximum differences of the orders of magnitude equal to 10^{-3} p.u. for the phase magnitudes, and 10^{-1} deg for the phase angles are obtained. The comparison between PFPD_MCA and DGS gives maximum mismatches of 10^{-3} p.u. for the three phase magnitudes, and 10^{-1} deg for the three phase angles.

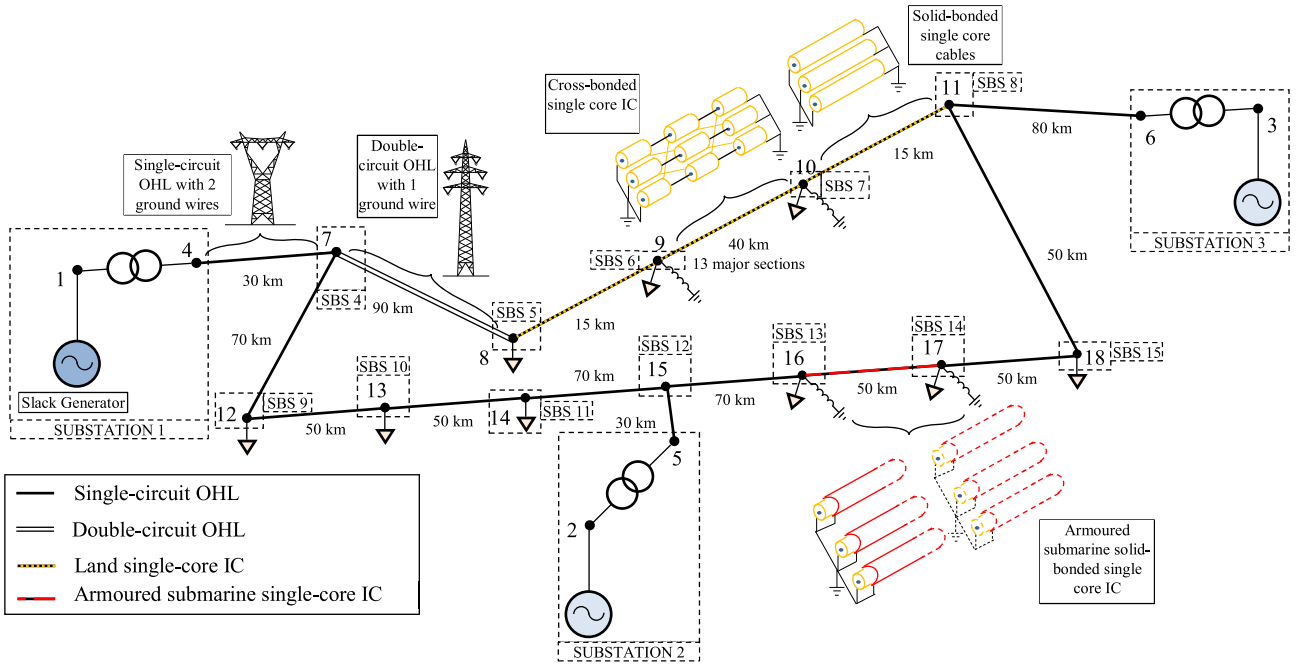

FIGURE 13. The 18-busbar case study.

TABLE 1. 18-busbar case study power losses computed with three different power flow algorithms: PFPD_MCA, the equivalent single-phase power-flow algorithm PFPD and the three-phase power flow commercial software DGS.

	PFPD_MCA	PFPD	DGS
Total Power Losses [MW]	*23.663*	*20.136*	*23.826*
Grid Reactive Power Absorption [Mvar]	*-217.6*	*-168.5*	*-217.49*

Such low differences confirm the result accuracy of PFPD_MCA.

The passive conductors of the AC electrical lines are subjected to induced voltages. Hence, depending on the adopted earthing method, induced currents can circulate in such conductors. These currents increase the power losses of the power system and their evaluation can be correctly assessed only by PFPD_MCA. In Tab. 1 the power loss comparison between PFPD_MCA and the equivalent single-phase PFPD is carried out: the network power losses estimated with PFPD_MCA are 15 % greater than the losses estimated with PFPD.

This difference is mainly due to the solid-bonded cables and the armour of the submarine cable. Differently from the other power flow algorithms, PFPD_MCA allows estimating power losses thoroughly and correctly. Furthermore, also the network reactive power can be computed with more accuracy, in fact, the reactive power absorption with the multiconductor approach is almost 50 Mvar greater than the equivalent single-phase one. This is due the exact representation of the electrical lines by means of MCA method, so the line admittances incorporate the interaction between the active and the passive conductors and the structural asymmetries.

The three-phase power flow algorithm implemented in the commercial software DGS considers the passive conductors installed in the electrical lines (such as earth wires of OHLs, screens and armours of IC lines) by means of Kron's reduction technique. This approach allows englobing in the active conductors the effects of the passive conductors. In Tab. 1 the power loss comparison between PFPD_MCA and the commercial software DGS is reported. The power losses obtained with PDPF_MCA differ by 160 kW for the Joule power losses and 100 kvar for the grid reactive power absorption. By considering the grid extension (*i.e.*, 760 km of transmission lines), the power mismatches confirm the method validity.

No power flow algorithm allows evaluating the electrical quantity behaviours along the electrical lines. Differently, after the power flow convergence, starting from the busbar voltages, PFPD_MCA determines the electrical quantity behaviours along the lines. This evaluation is fundamental to perform safety and electromagnetic compatibility considerations of the electrical lines. Fig. 14 shows the voltage magnitudes of all the conductors of the armoured submarine single core cable line interconnecting the nodes 16 and 17. The first diagram represents the phase to ground voltage magnitudes of the three active conductors along the 50 km link. The second diagram represents the screen voltage magnitudes along the cable.

The screens are earthed at the armour wires every 5 km, hence the screen voltages zero every 5 km. In real installations, it may happen that the earthed section lengths are unequal: PFPD_MCA suits very well also for this possibility. Eventually, the last diagram of Fig. 14 represents the armour

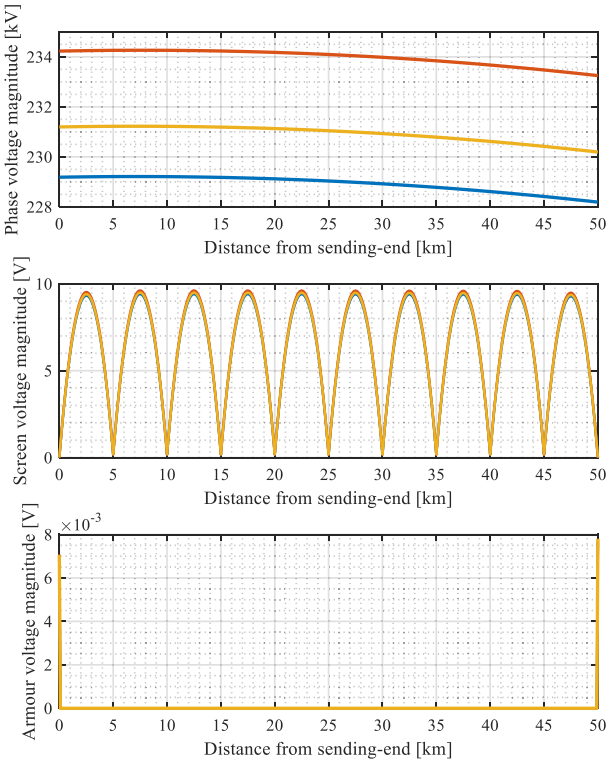

FIGURE 14. Voltage magnitude behaviours along the armoured submarine single-core IC conductors: phase conductors, screens and armours.

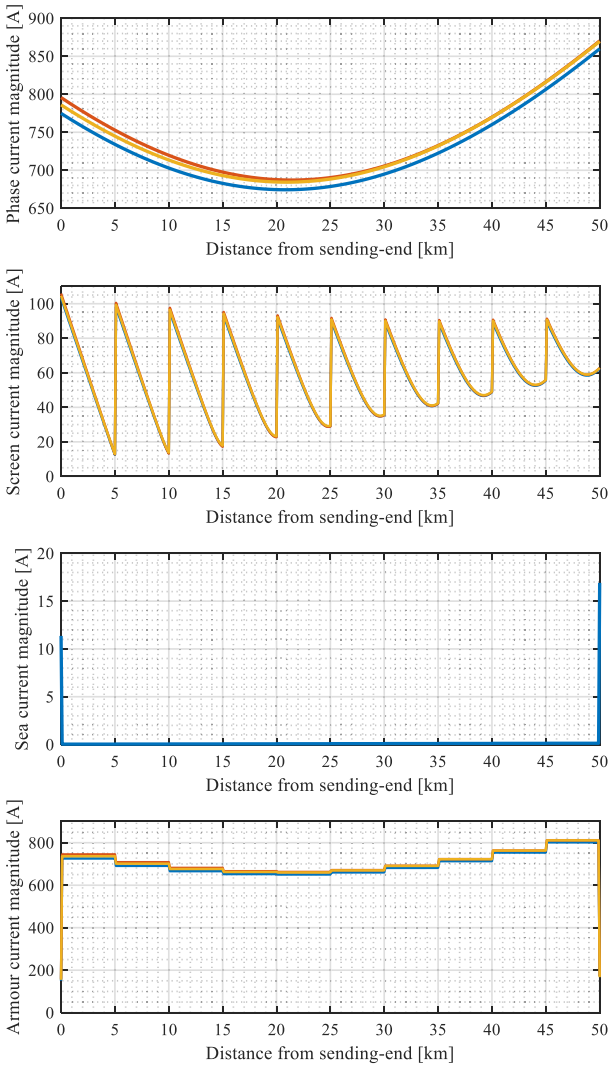

FIGURE 15. Current magnitude behaviour along the armoured submarine single-core IC: phase conductors, screen, armours and the stray current in the sea.

voltage magnitude of the three cables. Since the armour wires are in full contact with the sea water, their voltages are extremely low. Fig. 15 shows the current magnitude in all the conductors of the armoured submarine single-core IC line and also the stray currents in the sea. It is worth noting that the induced currents in the armours have a maximum value of 800 A.

In PFPD_MCA, the passive conductors are faithfully modelled along the electrical lines and also in the electrical substations. Therefore, it is possible to compute the passive conductor voltage in all the network busbars. Fig. 16 shows the passive conductor voltage magnitude in all the network busbars, both in absolute value and in per unit one. Busbar 1 and 4 are located in the same electrical substation (*i. e.*, Substation 1): in fact, they have the same absolute voltage magnitude, equal to 3.82 V.

Busbar 1 has a per unit voltage higher than busbar 4, since the first busbar has a nominal voltage lower than the second one. This confirms the correctness of the approach previously presented in Sect. III. The same consideration can be performed also between the busbars 2 and 5 or between the busbars 3 and 6.

The first two are both installed in the substation 2 and the latter two are located in the substation 3.

B. THE 39-SECTION NETWORK

The present technique is also applied to a 39-busbar network. This network is based on the standard New England IEEE 39-bus system. The system consists of 10 generators, 39 sections and 12 transformers. The considered grid has got the same topology of the reference grid, but the transmission line technologies are modified to show PFPD_MCA potential: OHLs, both single and double circuit, and underground IC lines are considered in the network. The power flow results obtained with PFPD_MCA are compared with the equivalent single-phase ones. Also for this network, small differences between the two methods are found by comparing the positive sequence quantities. The maximum differences are in the order of magnitude equal to 10^{-3} p.u. for the phase magnitudes, and 10^{-1} deg for the phase angles. As in the previous 18-section network, the network power losses computed with PFPD_MCA are 8.6 % greater than the losses computed with the equivalent single-phase method, *i. e.*, 28.08 MW versus 25.66 MW in the equivalent single-phase network. Furthermore, also the network reactive power computed with PFPD_MCA is greater than the same quantity estimated

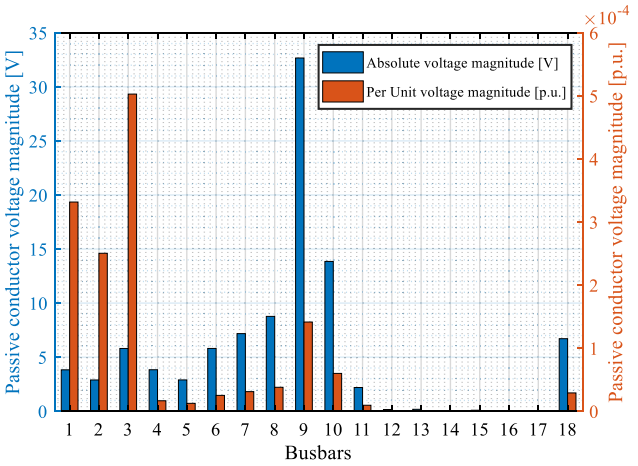

FIGURE 16. Passive conductor voltage magnitudes in the network nodes. The blue bars represent the absolute voltage magnitudes, instead, the orange bars represent the per unit voltage magnitudes.

TABLE 2. CPU-times and number of iterations for PFPD_MCA and DGS with a maximum acceptable power flow mismatch of 1 kVA for DGS and a maximum positive sequence voltage tolerance of 1 mV for PFPD_MCA.

	PFPD_MCA		DGS	
System	CPU time (ms)	ITER	CPU time (ms)	ITER
18 sections	1.3	6	40	5
39 sections	3	8	79	4

with PFPD. In fact, the multiconductor grid absorb 14 % more capacitive reactive power than the single-phase grid (−885 Mvar versus −759 Mvar in the equivalent single-phase network). The comparison between PFPD_MCA and the commercial software DGS shows maximum differences of 10^{-4} p.u. for the three phase magnitudes, and 10^{-2} deg for the three phase angles.

These differences are graphically shown in Fig. 17. The network power losses of the two methods differs by hundreds of kW, *i.e.*, 28.74 MW for PFPD_MCA compared with 28.44 MW of DGS. A similar result is obtained for the network reactive power absorption, in fact, a difference lower than 1 % can be computed (−885 Mvar versus −878 Mvar in the commercial software DGS). Table 2 compares the number of iterations (ITER) and the CPU-time of PFPD_MCA and DGS for both the considered case studies (18 and 39 section networks). The convergence criterion adopted by PFPD_MCA is a maximum positive sequence voltage tolerance of 1 mV, whereas, in DGS a maximum acceptable power flow mismatch of 1 kVA is imposed. Although the ITERs are greater in PDPD_MCA than DGS, the CPU times are always lower.

In order to have a safe power system operation, the electrical quantities should respect the equipment limit and the grid code. By exploiting PFPD_MCA, the electrical quantities in the network sections and along the lines can be assessed.

Figs. 18 and 19 show the voltage and the current magnitudes in all the conductors of a 18 km long cross-bonded

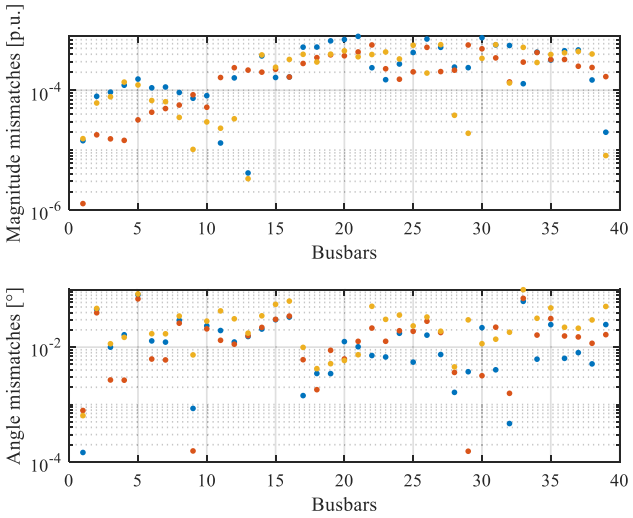

FIGURE 17. Magnitude and angle displacement in the 39-section grid. The blue dots represent the phase A, the orange dots represent the phase B and yellow ones the phase C.

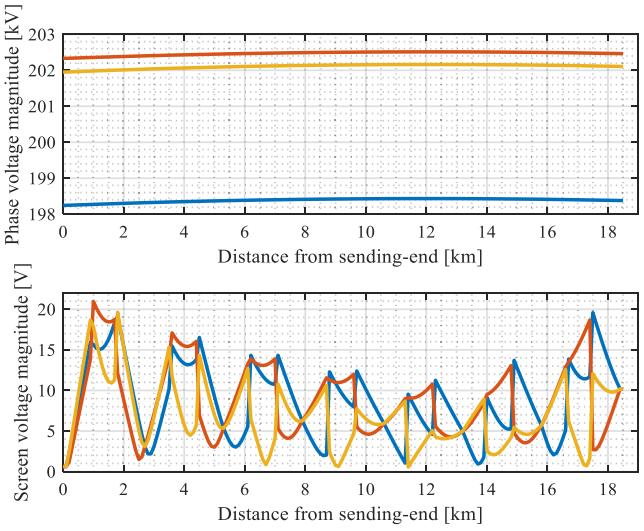

FIGURE 18. Voltage magnitude behaviour along cross-bonded single core IC conductors: phase conductors, screens.

IC. The 2500 mm^2 single-core IC has seven major sections, all with the same length. The unbalanced voltages, evaluated by the multiconductor power flow algorithm, are applied at the line ends; consequently, the voltages along the line are assessed. The method evaluates how the network unbalances impact on the line electrical quantities.

In this IC, the unbalance of the end section voltages causes the circulation of unbalanced currents in the active conductors.

Although the cross-bonding sections have equal lengths, currents and voltages are induced in the cable screens due to the unbalances in active conductor quantities. Differently from the other methods, PFPD_MCA evaluates how the network unbalanced elements interact each other. It also helps DSO/TSO to monitor whether the power system is being

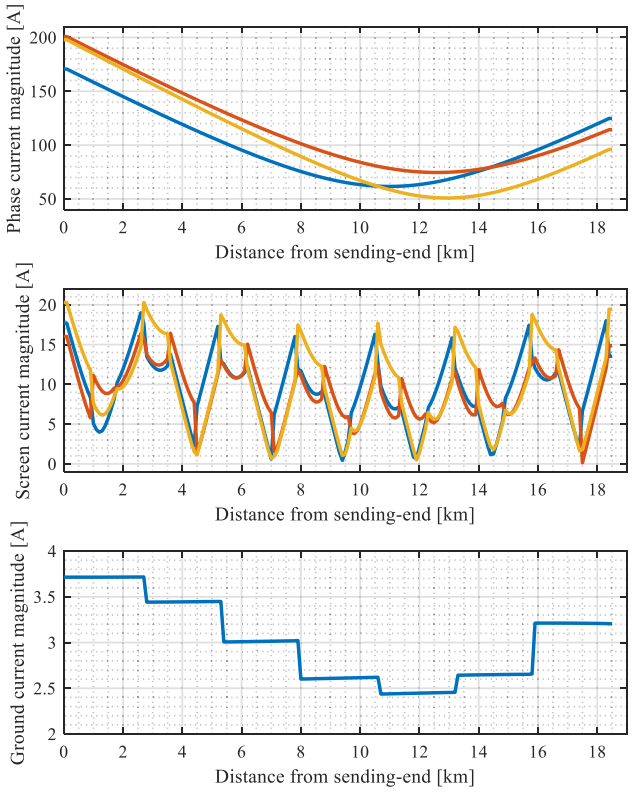

FIGURE 19. Current magnitude behaviour along cross-bonded single core IC conductors: phase conductors, screens and stray currents in the ground.

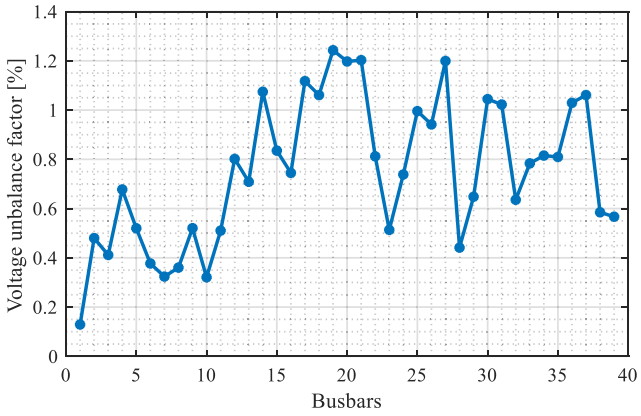

FIGURE 20. Voltage unbalance factor representation of the 39-section network.

operated within equipment and safety limits. The voltage unbalances may lead to the onset of unwanted phenomena like untimely grid protection interventions, and electrical machine overheating, which cause a systematic lowering in reliability, quality, and efficiency of the entire power system. This importance is highlighted in the international standards and reports [37], [38] which specify a "maximum voltage unbalance limit of 2% based on the 95-percentile of the 10-minute average measurements over at least one week". PFPD_MCA can be applied to foresee the voltage unbalance factors in all the network sections and model how different mitigation strategies can be implemented to reduce these voltage unbalance factors. Fig.20 shows the voltage unbalance factor in the 39-busbars of the network. The voltage unbalance factor in all the busbars is lower than the limit reported in [37]. Nevertheless, in some Countries the TSOs set a more severe limit for the voltage unbalance factor. For instance, the Italian TSO, Terna S.p.A., imposes a limit of 1 % for the voltage unbalance factor under normal conditions [39]; in this second case, the voltage unbalance factor of some sections exceeds the Italian TSO limit.

V. CONCLUSION

This paper presents a new multiconductor power flow algorithm. The algorithm, based on the admittance matrix, computes also the electrical quantities of the passive conductors of the electrical lines, *i. e.*, OHL ground wires, IC metallic screens/armours and GIL enclosures. Differently from the other algorithms, in PFPD_MCA the electrical line passive conductors are considered in the network admittance matrix. The method exploits a hybrid approach based on the simultaneous use of phase and sequence component frames of reference to solve the power flow problem. The passive conductors are correctly modelled both in the electrical substations and along the electrical lines. In fact, in the electrical substations, the connections between the different passive conductors are considered. Furthermore, all the conductors are connected to the corresponding resistance to earth of the meshed earth electrode. In order to represent the electrical lines, the MCA algorithm is employed. Each line is represented by considering its real laying configuration and conductor characteristics. The method is applied to two different case studies: an 18-busbar 380 kV network, and a 39-busbar one. The PFPD_MCA validation is carried out by means of comparisons with the equivalent single-phase power flow algorithm PFPD and also with the three-phase power flow solver of the commercial software DGS. In both case studies, PFPD_MCA evaluates the electrical quantities with more accuracy than PFPD and DGS. By this new PFPD_MCA, a power quality assessment of the distribution/transmission network can be performed limited to the evaluation of unbalance factors, power losses, also considering the passive conductors (*e. g.*, armours of submarine IC lines). Starting from their knowledge, TSOs can implement mitigation strategies to reduce the network unbalances. Furthermore, by exploiting a matrix technique, the electrical quantities along the lines can be also evaluated for all the conductors.

The knowledge of the electrical quantities along the lines can be adopted for different purposes:

- The voltages and the currents are useful for live line works;
- The currents in all the conductors (both the active and the passive ones) can be used to study the magnetic fields along all the line, and the ground return current (also

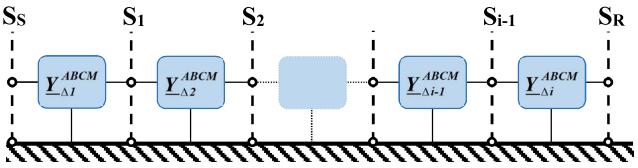

FIGURE 21. Elementary cells representation for a generic electrical line.

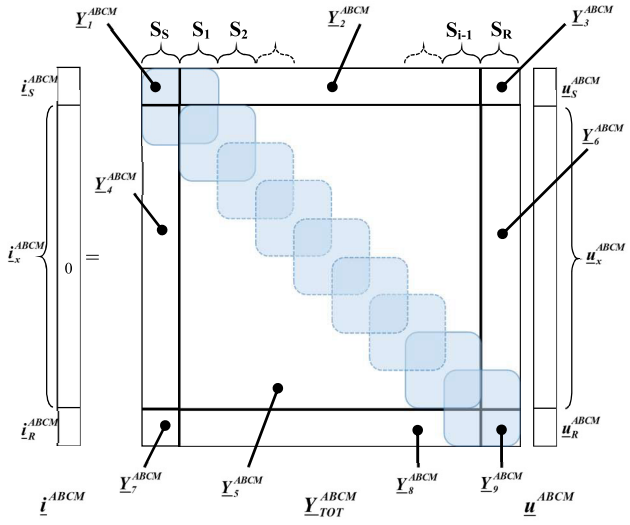

FIGURE 22. Structure of matrix $\underline{Y}_{TOT}^{ABCM}$, and partitioned matrix form of $\underline{i}^{ABCM} = \underline{Y}_{TOT}^{ABCM}\,\underline{u}^{ABCM}$.

known as stray current in the earth) or alternatively sea return current;

- The electrical quantities can be adopted to monitor whether the electrical lines, and in general the power system, are operated respecting equipment limits.

Future investigations are ongoing to solve the multiconductor power flow of real networks, *e.g.*, Italian transmission network.

APPENDIX

After the multiconductor power flow convergence, in PFPD_MCA the behaviour of the electrical quantities along the transmission lines can be determined. Starting from the voltages at end busbars of the considered line, the following method is applied. Once the $\underline{Y}_{\Delta}^{ABCM}$ matrix of all the elementary cells along the lines are computed, as in (11), it is necessary to achieve the admittance matrix $\underline{Y}_{TOT}^{ABCM}$ of the whole electrical line shown in Fig. 21 (where $\mathbf{S}_S, \mathbf{S}_R$ indicate the sending and the receiving end sections and $\mathbf{S}_1, \mathbf{S}_2, \ldots, \mathbf{S}_{i-1}$ indicate the ports along the electrical line). The building of the admittance matrix $\underline{Y}_{TOT}^{ABCM}$ involves all the matrices in Fig. 21 starting from the left side. $\underline{Y}_{TOT}^{ABCM}$ is calculated by using automatic topological procedures that give rise to partial superposition of matrices as in Fig. 22. The resulting matrix $\underline{Y}_{TOT}^{ABCM}$ can be of large dimensions (depending upon the ratio line length/Δ) but it can be easily managed because of it is structurally sparse. For the system of Fig 21, the general equation $\underline{i}^{ABCM} = \underline{Y}_{TOT}^{ABCM}\,\underline{u}^{ABCM}$ can be partitioned as in Fig 22.

It is worth noting that only $\underline{i}_S^{ABCM}$ and $\underline{i}_R^{ABCM}$ are non-zero current vectors and that $\underline{i}_x^{ABCM} \equiv 0$, it follows:

$$\begin{aligned}
\underline{i}_S^{ABCM} &= \underline{Y}_1^{ABCM} \cdot \underline{u}_S^{ABCM} + \underline{Y}_2^{ABCM} \cdot \underline{u}_x^{ABCM} + \underline{Y}_3^{ABCM} \cdot \underline{u}_R^{ABCM} \\
\underline{i}_x^{ABCM} &= \underline{Y}_4^{ABCM} \cdot \underline{u}_S^{ABCM} + \underline{Y}_5^{ABCM} \cdot \underline{u}_x^{ABCM} + \underline{Y}_6^{ABCM} \cdot \underline{u}_R^{ABCM} \\
\underline{i}_R^{ABCM} &= \underline{Y}_7^{ABCM} \cdot \underline{u}_S^{ABCM} + \underline{Y}_8^{ABCM} \cdot \underline{u}_x^{ABCM} + \underline{Y}_9^{ABCM} \cdot \underline{u}_R^{ABCM}
\end{aligned}$$

From the second equation, it is immediate to obtain the unknown voltage vector $\underline{u}_x^{ABCM}$:

$$\underline{u}_x^{ABCM} = -\left(\underline{Y}_5^{ABCM}\right)^{-1} \cdot \left(\underline{Y}_4^{ABCM} \cdot \underline{u}_S^{ABCM} + \underline{Y}_6^{ABCM} \cdot \underline{u}_R^{ABCM}\right)$$

where $\underline{Y}_5^{ABCM}$ is non singular. By knowing all the subvectors $\underline{u}_1^{ABCM}, \underline{u}_2^{ABCM}, \ldots, \underline{u}_{i-1}^{ABCM}$ of $\underline{u}_x^{ABCM}$, the steady-state regime of each cell is completely available. In this way, all the electrical quantities are known for each cell length.

REFERENCES

[1] W. F. Tinney and C. E. Hart, "Power flow solution by Newton's method," *IEEE Trans. Power App. Syst.*, vol. PAS-86, no. 11, pp. 1449–1460, Nov. 1967.

[2] B. Stott and O. Alsac, "Fast decoupled load flow," *IEEE Trans. Power App. Syst.*, vol. PAS-93, no. 3, pp. 859–869, May 1974, doi: 10.1109/TPAS.1974.293985.

[3] M. Baradar and M. R. Hesamzadeh, "AC power flow representation in conic format," *IEEE Trans. Power Syst.*, vol. 30, no. 1, pp. 546–547, Jan. 2015.

[4] S. D. Manshadi, G. Liu, M. E. Khodayar, J. Wang, and R. Dai, "A convex relaxation approach for power flow problem," *J. Modern Power Syst. Clean Energy*, vol. 7, no. 6, pp. 1399–1410, Nov. 2019.

[5] C. Coffrin, H. L. Hijazi, and P. Van Hentenryck, "The QC relaxation: A theoretical and computational study on optimal power flow," *IEEE Trans. Power Syst.*, vol. 31, no. 4, pp. 3008–3018, Jul. 2016.

[6] P. A. N. Garcia, J. L. R. Pereira, S. Carneiro, V. M. da Costa, and N. Martins, "Three-phase power flow calculations using the current injection method," *IEEE Trans. Power Syst.*, vol. 15, no. 2, pp. 508–514, May 2000.

[7] P. R. Bijwe, B. Abhijith, and G. K. V. Raju, "Robust three phase fast decoupled power flow," in *Proc. IEEE/PES Power Syst. Conf. Expo.*, Seattle, WA, USA, Mar. 2009, pp. 1–5.

[8] J. Arrillaga and B. J. Harker, "Fast-decoupled three-phase load flow," *Proc. Inst. Electr. Engineers*, vol. 125, no. 8, pp. 734–740, Aug. 1978.

[9] H. Le Nguyen, "Newton-raphson method in complex form [power system load flow analysis]," *IEEE Trans. Power Syst.*, vol. 12, no. 3, pp. 1355–1359, Aug. 1997.

[10] X.-P. Zhang, P. Ju, and E. Handschin, "Continuation three-phase power flow: A tool for voltage stability analysis of unbalanced three-phase power systems," *IEEE Trans. Power Syst.*, vol. 20, no. 3, pp. 1320–1329, Aug. 2005.

[11] I. Dzafic and H.-T. Neisius, "Generic three-phase power flow methods using symmetrical components for symmetrical and unsymmetrical power system networks," in *Proc. ISGT*, Anaheim, CA, USA, Jan. 2011, pp. 1–6.

[12] M. Abdel-Akher, K. M. Nor, and A. H. A. Rashid, "Improved three-phase power-flow methods using sequence components," *IEEE Trans. Power Syst.*, vol. 20, no. 3, pp. 1389–1397, Aug. 2005, doi: 10.1109/TPWRS.2005.851933.

[13] V. C. Strezoski and L. D. Trpezanovski, "Three-phase asymmetrical load-flow," *Int. J. Electr. Power Energy Syst.*, vol. 22, no. 7, pp. 511–520, Oct. 2000.

[14] X.-P. Zhang and H. Chen, "Sequence-decoupled Newton–Raphson three phase load flow," in *Proc. IEEE Region 10 Int. Conf. Comput., Commun. Autom. (TENCON)*, Beijin, China, Oct. 1993, pp. 394–397.

[15] X. Yang, Z. Wei, G. Sun, Y. Sun, Y. Yuan, Z. Lu, X. Xu, and L. Huang, "Power flow calculation for unbalanced three-phase distribution network with DGs based on phase-sequence hybrid modeling," in *Proc. IEEE Int. Conf. Smart Energy Grid Eng. (SEGE)*, Oshawa, ON, Canada, Aug. 2013, pp. 1–6, doi: 10.1109/SEGE.2013.6707926.
[16] B.-K. Chen, M.-S. Chen, R. R. Shoults, and C.-C. Liang, "Hybrid three phase load flow," *IEE Proc. C Gener., Transmiss. Distrib.*, vol. 137, no. 3, pp. 177–185, 1990.
[17] R. Benato, G. Gardan, and L. Rusalen, "A three-phase power flow algorithm for transmission networks: A hybrid phase/sequence approach," *IEEE Access*, vol. 9, pp. 162633–162650, 2021, doi: 10.1109/ACCESS.2021.3131778.
[18] F. M. Camilo, M. E. Almeida, R. Castro, and V. F. Pires, "Multi-conductor line models for harmonic load-flow calculations in LV networks with high penetration of PV generation," *J. Mod. Power Syst. Clean Energy*, vol. 10, no. 5, pp. 1288–1301, Sep. 2022, doi: 10.35833/MPCE.2020.000740.
[19] R. M. Ciric, A. P. Feltrin, and L. F. Ochoa, "Power flow in four-wire distribution networks-general approach," *IEEE Trans. Power Syst.*, vol. 18, no. 4, pp. 1283–1290, Nov. 2003, doi: 10.1109/TPWRS.2003.818597.
[20] L. R. Araujo, D. R. Penido, S. Carneiro, J. L. Pereira, and P. A. Garcia, "A comparative study on the performance of TCIM full Newton versus backward-forward power flow methods for large distribution systems," in *Proc. IEEE Power Energy Soc. Power Syst. Conf. Expo.*, Oct. 2006, pp. 522–526.
[21] D. Penido, L. Araujo, J. Pereira, P. Garcia, and S. Carneiro, "Four wire Newton–Raphson power flow based on the current injection method," in *Proc. IEEE Power Energy Soc. Power Syst. Conf. Expo.*, vol. 1, Oct. 2004, pp. 239–242.
[22] A. Heidari-Akhijahani, A. Safdarian, and M. Vrakopoulou, "A linear AC power flow model for unbalanced multi-phase distribution networks based on current injection equations," *IEEE Trans. Power Syst.*, vol. 36, no. 4, pp. 3806–3809, Jul. 2021, doi: 10.1109/TPWRS.2021.3073839.
[23] K. Sunderland, M. Coppo, M. Conlon, and R. Turri, "A correction current injection method for power flow analysis of unbalanced multiple-grounded 4-wire distribution networks," *Electr. Power Syst. Res.*, vol. 132, pp. 30–38, Mar. 2016, doi: 10.1016/j.epsr.2015.10.027.
[24] L. Sun, Y. Ju, L. Yang, S. Ge, Q. Fang, and J. Wang, "Holomorphic embedding load flow modeling of the three-phase active distribution network," in *Proc. Int. Conf. Power Syst. Technol. (POWERCON)*, Guangzhou, China, Nov. 2018, pp. 488–495, doi: 10.1109/POWERCON.2018.8602144.
[25] L. R. D. Araujo, D. R. R. Penido, and F. D. A. Vieira, "A multiphase optimal power flow algorithm for unbalanced distribution systems," *Int. J. Electr. Power Energy Syst.*, vol. 53, pp. 632–642, Dec. 2013, doi: 10.1016/j.ijepes.2013.05.028.
[26] S. Claeys, F. Geth, and G. Deconinck, "Optimal power flow in four-wire distribution networks: Formulation and benchmarking," *Electric Power Syst. Res.*, vol. 213, Dec. 2022, Art. no. 108522, doi: 10.1016/j.epsr.2022.108522.
[27] R. C. Dugan and T. E. McDermott, "An open source platform for collaborating on smart grid research," in *Proc. IEEE Power Energy Soc. Gen. Meeting*, Jul. 2011, pp. 1–7.
[28] G. Kron, "Compound *n*-matrices," in *Tensors for Circuits*, 2nd ed. New York, NY, USA: Dover, 1959, pp. 14–20.
[29] R. Benato, "Multiconductor analysis of underground power transmission systems: EHV AC cables," *Electr. Power Syst. Res.*, vol. 79, no. 1, pp. 27–38, Jan. 2009.
[30] C. R. Paul, *Analysis of Multiconductor Transmission Lines*. New York, NY, USA: Wiley, 1994.
[31] N. Pfeifer, M. Kizilcay, and P. Malicki, "Characteristics of a mixed 100-km EHV transmission line with shunt compensation for various topologies," in *Proc. 57th Int. Universities Power Eng. Conf. (UPEC)*, Istanbul, Turkey, Aug. 2022, pp. 1–6, doi: 10.1109/UPEC55022.2022.9917912.
[32] R. Benato, "A basic AC power flow based on the bus admittance matrix incorporating loads and generators including slack bus," *IEEE Trans. Power Syst.*, vol. 37, no. 2, pp. 1363–1374, Mar. 2022, doi: 10.1109/TPWRS.2021.3104097.
[33] R. Benato, G. Gardan, and A. Paolucci, "Power flow solution in asymmetrical multiconductor systems," *L'Energia Elettrica*, vol. 98, no. 2, pp. 1–12, Mar. 2021.
[34] F. Milano, "Power flow analysis," in *Power System Modeling and Scripting* (Power Systems Series). London, U.K.: Springer-Verlag, 2010, pp. 79–82.
[35] *Earthing of Power Installations Exceeding 1 KV A.C.*, IEC Standard 50522, 2022.
[36] R. Benato, S. Dambone Sessa, R. De Zan, M. R. Guarniere, G. Lavecchia, and P. S. Labini, "Different bonding types of Scilla–Villafranca (Sicily–Calabria) 43-km double-circuit AC 380-kV submarine–land cables," *IEEE Trans. Ind. Appl.*, vol. 51, no. 6, pp. 5050–5057, Nov. 2015, doi: 10.1109/TIA.2015.2448676.
[37] *Voltage Characteristics of Electricity Supplied by Public Distribution Systems*, IEC Standard 50160, 2010.
[38] F. Ghassemi and M. Perry, "Review of voltage unbalance limit in the GB grid code CC.6.1.5 (b)," GCRP, Nat. Grid, London, U.K., Nov. 2014. [Online]. Available: http://www.nationalgrid.com/sites/default/files/documents/37643-Voltage%20Unbalance%20Report.pdf
[39] *Connection to the National Electricity Transmission System in Grid Code* (Accesso Alla Rete di Trasmissione Nazionale in Codice di Rete), Terna, Rome, Italy, 2004.

LUCA RUSALEN (Member, IEEE) was born in Treviso, Italy, in 1996. He received the bachelor's and Dr.-Ing. degrees in energy engineering from the University of Padova, in 2019 and 2021, respectively. He is currently pursuing the Ph.D. degree in industrial engineering. His research interests include computer analysis of power systems and transmission line modeling. He is an AEIT Young Member.

ROBERTO BENATO (Senior Member, IEEE) was born in Venezia, Italy, in 1970. He received the Dr.Ing. degree in electrical engineering from the University of Padova, Padua, Italy, in 1995, and the Ph.D. degree in power systems analysis, in 1999. In 2021, he was a Full Professor with the Department of Industrial Engineering, University of Padova. He is the author of 250 articles and four books, edited by Springer, Wolters Kluwer, Amazon KDP, and China Machine Press. He has been a member of the Six Cigré Working Groups (WGs) and the Secretary of the Two Joint WGs. He is a member of the IEEE PES Substations Committee. In 2014, he was nominated as a member of IEC TC 120 "Electrical Energy Storage (EES) Systems" in the WG 4 "Environmental Issues of EES Systems." He is a Corresponding Member of Cigré WG B1.72 "Cable Rating Verification Second Part." In 2018, he has been elevated to the grade of CIGRÉ Distinguished Member. He is a member of Italian AEIT.

Open Access funding provided by 'Università degli Studi di Padova' within the CRUI CARE Agreement